J. Fluid Mech. (1989), vol. 207, pp. 587–628
Printed in Great Britain

Nonlinear compressible magnetoconvection Part 1. Travelling waves and oscillations

By N. E. HURLBURT, M. R. E. PROCTOR, N. O. WEISS AND D. P. BROWNJOHN

Department of Applied Mathematics and Theoretical Physics, University of Cambridge, Silver Street, Cambridge CB3 9EW, UK

(Received 31 October 1988 and in revised form 3 May 1989)

Two-dimensional compressible convection in a polytropic layer with an imposed vertical magnetic field is studied in a series of numerical experiments. We consider a shallow layer, spanning only a fraction of a scale height in density, and increase the ratio (β^{-1}) of the magnetic to the thermal pressure in a regime where convection sets in at an oscillatory bifurcation. Initially there are stable periodic oscillations (standing wave solutions). For moderate values of β the only deviations from Boussinesq behaviour are where the field is locally intense but as β is decreased magnetic pressure fluctuations become increasingly important. When β is of order unity at the top of the layer standing waves become unstable at higher Rayleigh numbers and travelling waves are preferred. This is an essentially compressible effect in which magnetic pressure plays a crucial role. The associated bifurcation structure is investigated in some detail.

1. Introduction

Strong magnetic fields inhibit convection at the surfaces of stars with deep convective envelopes. Isolated flux tubes therefore coincide with cooler, darker patches and these spots are the most prominent signs of magnetic activity in stars like the Sun. The existence of sunspots and starspots has motivated detailed studies of magnetoconvection, mainly within the framework of the Boussinesq approximation. Investigations of linear and nonlinear behaviour have confirmed that steady overturning convection is suppressed by strong magnetic fields (Chandrasekhar 1961; Cowling 1976; Proctor & Weiss 1982). However, oscillatory convection may still occur if the ratio ζ of the magnetic to the thermal diffusivity is sufficiently small. This condition is satisfied in sunspot umbrae, where heat transport requires some form of time-dependent motion. Since stellar atmospheres are compressible it is important to relax the constraints imposed by the Boussinesq approximation and recent studies have explored both the effects of stratification and the role of local or global increases in magnetic pressure (Hughes & Proctor 1988). We shall investigate fully compressible time-dependent behaviour.

Nonlinear treatments inevitably lead to large-scale numerical computation. Here there are two possible approaches. The first is to represent stellar processes in as much detail as possible. Thus Nordlund (1984, 1985) has simulated the interaction between convection and weak magnetic fields in the solar photosphere, while others have modelled stellar dynamos in spherical geometry (Moss 1986). The alternative is to construct idealized fluid dynamical problems that allow us to isolate individual effects and to investigate them in some detail. We prefer the latter approach. This

paper demonstrates that by systematically varying the parameters in idealized numerical experiments we can not only recognize different physical processes but also identify specific bifurcations which can be related to recent developments in nonlinear dynamics (Guckenheimer & Holmes 1983). Moreover, our results are relevant to other examples of double convection, with applications in the laboratory and the oceans as well as to astrophysics.

In the absence of any dissipation a vertical magnetic field supports fast and slow magnetoacoustic waves in an unstratified layer. These waves differ not only in phase speed but also in the relative importance of the compressional and vortical components of the motion. A necessary condition for the Boussinesq approximation to be valid is that the ratio β of thermal pressure to magnetic pressure should be large; in that case the fast waves are just sound waves, which travel isotropically, while slow waves travel along the magnetic field with the Alfvén speed as transverse hydromagnetic waves. At the other extreme, when $\beta \ll 1$, fast magnetoacoustic waves travel isotropically with the Alfvén speed, while slow waves are purely compressional and propagate along the field at the sound speed (Priest 1982). In a weakly stratified layer such waves may become unstable in the presence of diffusion. In the Boussinesq limit slow magnetoacoustic waves are coupled to the thermal stratification, which can maintain oscillatory (overstable) motion against ohmic and viscous dissipation provided that $\zeta < 1$. When $\beta \ll 1$ the slow waves again become unstable in a superadiabatic temperature gradient. As β passes through unity there is a change in the convective modes from motion across the field to predominantly vertical motion along the field lines. Behaviour is more complicated for β of order unity, when fast and slow magnetoacoustic modes have similar speeds and are strongly coupled by the stratification (Cattaneo 1984; Hughes & Proctor 1988). The onset of oscillatory convection in a polytropic atmosphere has been investigated by Antia & Chitre (1979) and Cattaneo (1984). In this paper we explore behaviour in the nonlinear regime and show that compressibility leads to the appearance of stable travelling waves when β is of order unity.

Two-dimensional compressible convection was studied numerically by Graham (1975) and Hurlburt, Toomre & Massaguer (1984). More recently, Hurlburt & Toomre (1988) have investigated nonlinear compressible magnetoconvection in a series of numerical experiments that has greatly extended our understanding of the subject. They were mainly concerned with steady convection and focused particularly on the role of magnetic pressure P_m in the nonlinear regime. Even when β is large, so that magnetic pressure is unimportant in the absence of convection, convective eddies will concentrate magnetic flux into sheets where the field is locally intense and P_m becomes comparable with the thermal pressure P. Continuity of total pressure $\Pi = P + P_m$ then requires that P should decrease where P_m is large; thus flux sheets are partially evacuated and the density is reduced where the field is strong. Magnetic buoyancy therefore augments thermal buoyancy at the base of the layer (where motion converges on a rising plane) but opposes it at the top. Owing to stratification the latter effect is more important, so magnetic pressure cooperates with magnetic tension to hinder convection.

Hurlburt & Toomre surveyed a wide range of parameters but only described one example of oscillatory convection. In this series of papers we shall concentrate on time-dependent nonlinear magnetoconvection in a fully compressible fluid with $\zeta < 1$. We have carried out several sets of numerical experiments using a program similar to that of Hurlburt & Toomre (1988), which describes two-dimensional convection in a perfect gas with uniform properties. In these calculations we follow the evolution

of perturbations to a static polytropic atmosphere with prescribed polytropic index m and density contrast χ. The temperature is fixed at the upper and lower boundaries, where the vertical component of the velocity, the horizontal component of the magnetic field and the tangential component of the viscous stress all vanish. All quantities are assumed to be periodic in the horizontal direction, with wavelength λ. Then we obtain solutions for different values of the Rayleigh number $\hat{R}$ and the ratio $\hat{\beta} = \hat{P}/P_{\mathrm{m}}$, measured at the midpoint of a static layer.

In the first two papers we consider the effects of increasing the magnetic pressure in a weakly stratified atmosphere. Part 1 is concerned with the regime where convection sets in at an oscillatory bifurcation, allowing either standing wave or travelling wave solutions. Part 2 deals with the kinematic regime, where convection sets in at a stationary bifurcation but hydrodynamic instabilities lead to the appearance of travelling waves and oscillatory streaming motion, which interacts with the magnetic field. In the third paper (to be published elsewhere) we turn to a stratified layer with a density contrast $\chi = 11$ and a corresponding increase of ζ with depth, which models behaviour in the solar atmosphere.

In this paper, after setting up the problem, we study periodic oscillations in a box with aspect ratio $\lambda = 2$. We find that these standing wave solutions, with two square rolls, give way to travelling wave solutions with four rolls in the box as the Rayleigh number is increased. In order to explain this transition it is necessary to understand both the associated bifurcation structure and the dynamical effect of local increases in magnetic pressure. The interplay between mathematical and physical aspects of the problem is perhaps the most interesting feature of this study. Some preliminary results were published by Hurlburt & Weiss (1987) and reproduced by Hughes & Proctor (1988).

The equations governing two-dimensional compressible magnetoconvection are set out in the next section and reduced to dimensionless form. Nonlinear solutions are obtained numerically, using a two-step Lax–Wendroff scheme modified to allow semi-implicit treatment of diffusive terms. Linear stability is discussed in §3, where we show that deviations from Boussinesq results are relatively slight. Next, in §4, we consider standing wave solutions with aspect ratio $\lambda = 2$, comparing behaviour for $\hat{\beta} = 32$ (when magnetic pressure fluctuations are only locally important) with that for $\hat{\beta} = 8$, when magnetic buoyancy is dominant. In §5 we find that standing waves become unstable as $\hat{R}$ is increased for fixed $\hat{\beta} = 8$ and are replaced by travelling waves in which magnetic pressure fluctuations play a key role, though the waves travel with the same speed as slow magnetoacoustic modes in the Boussinesq approximation. Since the travelling waves appear with half the wavelength of the standing waves we consider the transition from standing waves to travelling waves with $\lambda = 1$ in §6, where we establish that stable travelling waves are a compressible phenomenon, appearing only for $\hat{\beta} \leqslant 32$. In §7 we explore the more complicated bifurcation patterns associated with a transition from two-roll standing wave solutions to four-roll travelling wave solutions when $\lambda = 2$. Finally we discuss the physical origin of the travelling wave solutions in the concluding section.

2. The two-dimensional problem

2.1. *The governing equations*

We shall consider convection in a plane parallel layer of compressible fluid in the presence of an externally imposed vertical magnetic field. The fluid occupies the region $0 < z < d$, referred to Cartesian axis with the z-axis pointing downwards. We

suppose that the velocity $\boldsymbol{u}$ and the magnetic field $\boldsymbol{B}$ lie in the (x,z)-plane and that no quantities vary in the y-direction. The fluid is assumed to be a perfect monatomic gas with constant heat capacities c_p and c_v, and the shear viscosity μ, the thermal conductivity K, the magnetic diffusivity η and the magnetic permeability μ_0 are also assumed to be constant. The density $\rho(x,z,t)$ satisfies the continuity equation

$$\frac{\partial \rho}{\partial t}+\boldsymbol{\nabla}\cdot(\rho\boldsymbol{u})=0 \tag{2.1}$$

and is related to the pressure P and the temperature T by the equation of state

$$P=R_*\rho T, \tag{2.2}$$

where R_* is the gas constant. It is helpful to express the remaining equations in conservative form (Graham 1975; Hurlburt *et al.* 1984; Hurlburt & Toomre 1988). The magnetic field is solenoidal, so that

$$\boldsymbol{\nabla}\cdot\boldsymbol{B}=0, \tag{2.3}$$

and satisfies the induction equation, which can be written in the form

$$\frac{\partial \boldsymbol{B}}{\partial t}+\boldsymbol{\nabla}\cdot\boldsymbol{L}=0, \tag{2.4}$$

where $\boldsymbol{L}$ is an antisymmetric matrix with elements

$$L_{ij}=u_jB_i-u_iB_j-\eta\left(\frac{\partial B_i}{\partial x_j}-\frac{\partial B_j}{\partial x_i}\right), \quad i,j=1,2,3 \tag{2.5}$$

and $(\boldsymbol{\nabla}\cdot\boldsymbol{L})_i=\partial L_{ij}/\partial x_j$ with $(x_1,x_2,x_3)=(x,y,z)$. The energy equation can also be written in conservative form as

$$\frac{\partial}{\partial t}\left[\rho(c_vT+\tfrac{1}{2}|\boldsymbol{u}|^2-gz)+\frac{1}{2\mu_0}|\boldsymbol{B}|^2\right]+\boldsymbol{\nabla}\cdot[\rho(c_pT+\tfrac{1}{2}|\boldsymbol{u}|^2-gz)\boldsymbol{u}-K\boldsymbol{\nabla}T+\boldsymbol{M}]=0, \tag{2.6}$$

where the vector $\boldsymbol{M}$ has components

$$M_i=u_i\tau_{ji}-\left(\frac{\eta}{\mu_0}\right)B_j\left(\frac{\partial B_i}{\partial x_j}-\frac{\partial B_j}{\partial x_i}\right)+\mu_0^{-1}B_j(B_iu_j-B_ju_i), \tag{2.7}$$

and the viscous stress tensor

$$\tau_{ij}=\mu\left(\frac{\partial u_i}{\partial x_j}+\frac{\partial u_j}{\partial x_i}-\tfrac{2}{3}\delta_{ij}\frac{\partial u_l}{\partial x_l}\right). \tag{2.8}$$

Finally, the equation of motion takes the form

$$\frac{\partial}{\partial t}\rho\boldsymbol{u}+\boldsymbol{\nabla}\cdot\boldsymbol{N}=0, \tag{2.9}$$

where $\boldsymbol{N}$ is a symmetric matrix with elements

$$N_{ij}=\left(P+\frac{B_kB_k}{2\mu_0}\right)\delta_{ij}+\rho u_iu_j-\frac{B_iB_j}{\mu_0}-\rho g x_3\delta_{ij}-\tau_{ij} \tag{2.10}$$

and g is the (constant) gravitational acceleration.

The equations (2.1)–(2.10) are solved in the rectangular region $\{0<x<\lambda d, 0<$

$z < d\}$ subject to appropriate boundary conditions. We assume that the temperature is fixed at the upper and lower boundaries, so that

$$T(x,0) = T_0, \quad T(x,d) = T_0 + \Delta T, \tag{2.11}$$

where ΔT is the temperature difference across the layer and T_0 is a constant. We further assert that the total magnetic flux through the region remains constant and that the horizontal component of the magnetic field vanishes on the upper and lower boundaries, so that

$$B_x = 0 \quad \text{at} \quad z = 0, d, \quad \int_0^{\lambda d} B_z \, \mathrm{d}x = B_0 \lambda d, \tag{2.12}$$

where B_0 is the magnitude of the uniform vertical magnetic field in the absence of convection. In addition we suppose that the vertical velocity and the tangential components of the viscous stress vanish at the upper and lower boundaries, so that

$$w = 0, \quad \frac{\partial u}{\partial z} = 0 \quad \text{at} \quad z = 0, d, \tag{2.13}$$

where $\boldsymbol{u} = (u, 0, w)$. Finally, we assume that all variables are periodic in x with period λd, so that $T(\lambda d, z, t) = T(0, z, t)$ etc.

In order to write the equations in dimensionless form we adopt the layer depth d as our unit of length and transfer the origin to the plane $z = -T_0 d/\Delta T$. Our unit of time is the reduced sonic travel time $(d^2/R_* \Delta T)^{\frac{1}{2}}$ and the density is scaled by the density ρ_0 at the top of the layer in the absence of convection. The temperature is scaled by the temperature difference ΔT across the layer and the magnetic field by B_0. The dimensionless thermal conductivity is then given by

$$\bar{K} = \frac{K}{c_p \rho_0 d (R_* \Delta T)^{\frac{1}{2}}}. \tag{2.14}$$

All variables will henceforth be displayed in dimensionless form. Then (2.2) reduces to $P = \rho T$ and (2.10) can be written as

$$N_{ij} = [P + \tfrac{1}{2} F B_k B_k] \delta_{ij} + \rho u_i u_j - F B_i B_j - (m+1) x_3 \delta_{ij} - \tau_{ij}, \tag{2.15}$$

where the strength of the magnetic field is measured by the dimensionless parameter

$$F = \frac{B_0^2}{\mu_0 R_* \rho_0 \Delta T} = \sigma \zeta_0 \bar{K}^2 Q \tag{2.16}$$

(the square of the ratio of the Alfvén speed to the reduced sound speed). Here the Chandrasekhar number

$$Q = \frac{B_0^2 d^2}{\mu_0 \mu \eta}, \tag{2.17}$$

and the Prandtl numbers

$$\sigma = \mu c_p / K, \quad \zeta_0 = \eta \rho_0 c_p / K. \tag{2.18}$$

measure the ratios of the viscous and magnetic diffusivities to the thermal diffusivity, while

$$m = \frac{gd}{R_* \Delta T} - 1 \tag{2.19}$$

is the polytropic index (see §2.2 below). In (2.5) and (2.8) η and μ are replaced by $\zeta_0\bar{K}$ and $\sigma\bar{K}$ respectively, while the energy equation (2.6) becomes

$$\frac{\partial}{\partial t}\left[\rho\left\{\frac{T}{\gamma-1}+\tfrac{1}{2}|\boldsymbol{u}|^2-(m+1)z\right\}+\tfrac{1}{2}F|\boldsymbol{B}|^2\right] + \boldsymbol{\nabla}\cdot\left[\rho\left(\frac{\gamma T}{\gamma-1}+\tfrac{1}{2}|\boldsymbol{u}|^2-(m+1)z\right)\boldsymbol{u}-\bar{K}\boldsymbol{\nabla}T+\boldsymbol{M}\right]=0, \quad (2.20)$$

where $\gamma = c_p/c_v$ and

$$M_i = -u_j\tau_{ij}+F\left[\zeta_0\bar{K}B_j\left(\frac{\partial B_i}{\partial x_j}-\frac{\partial B_j}{\partial x_i}\right)+B_j(B_j u_i-B_i u_j)\right]. \quad (2.21)$$

These dimensionless equations have to be solved in the domain $\{0<x<\lambda, z_0<z<z_0+1\}$, where $z_0 = T_0/\Delta T$. Thus the state of the system is described by the six physical parameters m, $\bar{K}$, z_0, F, σ and ζ_0, together with the aspect ratio λ.

2.2. *The static reference atmosphere*

The governing equations possess a trivial equilibrium solution describing a static, stratified layer with a uniform vertical magnetic field and heat transported entirely by conduction. The atmosphere is then a polytrope with

$$T = z, \quad \rho = \left(\frac{z}{z_0}\right)^m, \quad P = \frac{z^{m+1}}{z_0^m}, \quad (2.22)$$

where the polytropic index m was defined in (2.19). Hence the ratio of the density at the base of the layer to that at the top is given by the density contrast

$$\chi = \left(\frac{z_0+1}{z_0}\right)^m. \quad (2.23)$$

For an adiabatically stratified layer $m = 1/(\gamma-1)$; we shall consider a monatomic gas with $\gamma = \frac{5}{3}$, which is unstably stratified if $m < \frac{3}{2}$. The degree of instability may be measured by the Rayleigh number with a local value

$$R(z) = \left[\frac{g(\Delta T-gd/c_p)\,d^3}{T(\mu/\rho)\,(K/c_p\rho)}\right] = (m+1)\left\{1-\frac{\gamma-1}{\gamma}(m+1)\right\}\frac{z^{2m-1}}{\sigma\bar{K}^2 z_0^{2m}}, \quad (2.24)$$

where the quantities in *square* brackets are dimensional. Another important quantity is the ratio of the gas pressure to the magnetic pressure (or the thermal to the magnetic energy density)

$$\beta(z) = \left[\frac{2\mu_0 P}{B_0^2}\right] = \frac{2z^{m+1}}{Fz_0^m} = \frac{2z^{m+1}}{\sigma\zeta_0\bar{K}^2 Q z_0^m}. \quad (2.25)$$

This quantity is inversely proportional to the square of the ratio Φ of the Alfvén speed v_A to the sound speed v_S given by

$$\Phi(z) = \left[\frac{B_0^2}{\gamma\mu_0 P}\right]^{\frac{1}{2}} = \left(\frac{2}{\gamma\beta(z)}\right)^{\frac{1}{2}}. \quad (2.26)$$

Note that the local value of the magnetic Prandtl number is proportional to the density so that

$$\zeta(z) = \zeta_0\rho = \zeta_0\left(\frac{z}{z_0}\right)^m. \quad (2.27)$$

It is often convenient to use the properties of the static reference atmosphere to characterize the state of the system. This is particularly appropriate when considering linear stability (Spiegel 1964; Gough *et al.* 1976; Cattaneo 1984); it can then be shown that parameters evaluated in the middle of the layer can most readily be compared with Boussinesq calculations as $\chi \to 1$. We therefore define $\hat{R} = R(z_0+\frac{1}{2})$, $\hat{\beta} = \beta(z_0+\frac{1}{2})$, $\hat{\Phi} = \Phi(z_0+\frac{1}{2})$ and $\hat{\zeta} = \zeta(z_0+\frac{1}{2})$ and we use these quantities to describe the state of the convecting system. In practice many of our solutions have been obtained by solving the equations using the (unstable) reference atmosphere to provide initial conditions and introducing small velocity perturbations involving many lengthscales.

2.3. *Numerical methods*

Nonlinear numerical solutions are obtained for these two-dimensional flows using a two-step Lax–Wendroff scheme, modified to include diffusion of vorticity, magnetic field and heat. The basic approach follows that of Graham (1975). The Lax–Wendroff algorithm uses equations in a conservative form, much as equations (2.1)–(2.10) are written. In particular, the total mass of the system and the total horizontal momentum are exactly conserved. Further, since we solve for both components of $\boldsymbol{B}$ using the induction equation (2.4) in finite-difference form with an antisymmetric matrix $\boldsymbol{L}$, the total magnetic flux in the region is also conserved to machine accuracy. The time advance occurs in two steps and involves the use of two spatially staggered meshes. Since we are interested in solutions with small Prandtl numbers here, where the thermal diffusion time is much smaller than any other timescale, we solve the thermal equation using a semi-implicit scheme as discussed in the Appendix. The other equations are solved using the explicit Lax–Wendroff time scheme and thus Courant conditions based on advection, wave propagation and diffusion must still be satisfied in the choice of maximum time step. Most of the calculations described in this paper used a mesh with 40 points in the vertical direction and some results were verified by doubling the spatial resolution of the mesh. A typical run of 500 dimensionless time units took about 1 h on a Cray-1S computer.

3. Linear stability

In these two papers we shall restrict our attention to a fixed shallow reference atmosphere with $z_0 = \frac{1}{6}$ and a polytropic index $m = 0.25$. For this atmosphere the density contrast $\chi \approx 1.63$ and the density stratification is therefore relatively unimportant. In astrophysical terms, the ratio of the layer depth to the density scale height at the upper boundary is $m/z_0 = 1.5$ and the ratio to the pressure scale height is $(m+1)/z_0 = 7.5$.

The relative importance of the magnetic pressure is measured by the parameter F, which is inversely proportional to $\hat{\beta}$. For our choice of parameters $\hat{\beta} \approx 1.89/F$, from (2.25). In this paper we shall study the effect of increasing the magnetic pressure in the range $256 \geqslant \hat{\beta} \geqslant 6\,(0.007 < F < 0.32)$. Now the Boussinesq approximation is valid only if $F \ll 1$ (so that $v_A \ll v_S$) and $z_0 \gg m+1$ (whence it follows that $\chi \approx 1$). Studies of linear and nonlinear convection in the absence of a magnetic field suggest, however, that Boussinesq results may remain an adequate approximation for $\chi \lesssim 5$. As F is increased from zero the magnetic pressure becomes larger relative to the gas pressure. In the nonlinear regime regions with strong fields are partially evacuated. Deviations from Boussinesq behaviour are therefore to be expected as F approaches unity.

We first consider bifurcations from the static equilibrium solutions of §2.2 in order to determine the range of validity of the Boussinesq approximation. In the Boussinesq limit there is a stationary bifurcation when $R = R^{(e)}$, where

$$R^{(e)} = R_0 + \tfrac{1}{4}\pi^2(\lambda^2+4)\,Q \tag{3.1}$$

for rolls of width $\frac{1}{2}\lambda$ while $R_0 = \pi^4(\lambda^2+4)^3/4\lambda^4$ is the bifurcation value in the absence of a magnetic field. For $\zeta < 1$ and $Q > \pi^2(\lambda^2+4)^2\zeta(1+\sigma)/\lambda^4\sigma(1-\zeta)$ instability first sets in through a Hopf bifurcation at $R = R^{(o)}$, where

$$R^{(o)} = R_0\left[1+\frac{\zeta}{\sigma}(1+\sigma+\zeta)\right]+\frac{\zeta(\zeta+\sigma)\,\pi^2(\lambda^2+4)}{4(1+\sigma)}Q \tag{3.2}$$

(Chandrasekhar 1961; Proctor & Weiss 1982). Thus $R \propto Q$ for large Q at both bifurcation points.

We want to study the effect of increasing the Rayleigh number without changing the structure of the reference atmosphere. Thus we keep m and z_0 fixed and vary the heat flux by altering the dimensionless thermal conductivity $\bar{K}$; since we are concerned with oscillatory convection the values of σ and ζ_0 are held constant. Then it follows from (2.16) and (3.2) that for Q sufficiently large ($Q > 10^4$) the value of F at $R = R^{(o)}$ approaches a constant value of order unity, and the conditions for the Boussinesq approximation are therefore likely to be violated. Hence one must analyse the compressible system in order to understand behaviour at large Q. For the linear calculations described in this section we take $\zeta = \sigma = 0.1$. Figure 1(*a*) shows the values of $\hat{R}$ for the onset of steady ($\hat{R}^{(e)}$) and oscillatory ($\hat{R}^{(o)}$) convection as functions of the Chandrasekhar number Q for an aspect ratio $\lambda = 2$, calculated with the program developed by Cattaneo (1984). The broken curves indicate the values predicted by the Boussinesq expressions (3.1) and (3.2). Note that $\hat{R}^{(e)}$ is substantially greater than $\hat{R}^{(o)}$, since ζ is small and Q is relatively large. Although $\hat{R}^{(e)}$ is higher in the fully compressible case than in the Boussinesq limit, the two curves have the same limiting form.

In the parameter ranges with which we are concerned convection appears as an oscillatory instability and the Hopf bifurcation is apparently supercritical. At small Q the values of $R^{(o)}$ predicted by Boussinesq theory agree well with the fully compressible results. This confirms that oscillatory solutions will be insensitive to the variations in pressure and density across the layer; any deviations from Boussinesq behaviour must be caused by the large field strengths as F approaches unity. Such deviations appear for $Q > 10^3$, where the two curves begin to diverge significantly. At first $\hat{R}^{(o)}$ rises more slowly for compressible magnetoconvection than in the Boussinesq limit, suggesting the presence of some other driving mechanism. Then, for $Q > 10^4$, $\hat{R}^{(o)}$ increases more rapidly than $R^{(o)}$: for $Q \gg 10^4$ we find that $\hat{R}^{(o)} \propto Q^{1.14}$, while $R^{(o)} \propto Q$ from (3.2). We therefore find that $\hat{R}^{(o)} > R^{(o)}$ for $Q > 10^5$. Since $\hat{R}^{(o)}$ then increases more rapidly than $\hat{R}^{(e)}$ it is conceivable that steady convection may be preferred at very large Q for this aspect ratio. We shall not pursue this possibility here, instead concentrating on the region with $Q < 10^5$.

It is important to realize that $\hat{R}$, Q and F cannot be varied independently. From (2.16), (2.24) and (2.27)

$$F = (m+1)\left\{1-\frac{\gamma-1}{\gamma}(m+1)\right\}\frac{\hat{\zeta}Q}{\hat{R}}\frac{(z_0+\frac{1}{2})^{m-1}}{z_0^m}. \tag{3.3}$$

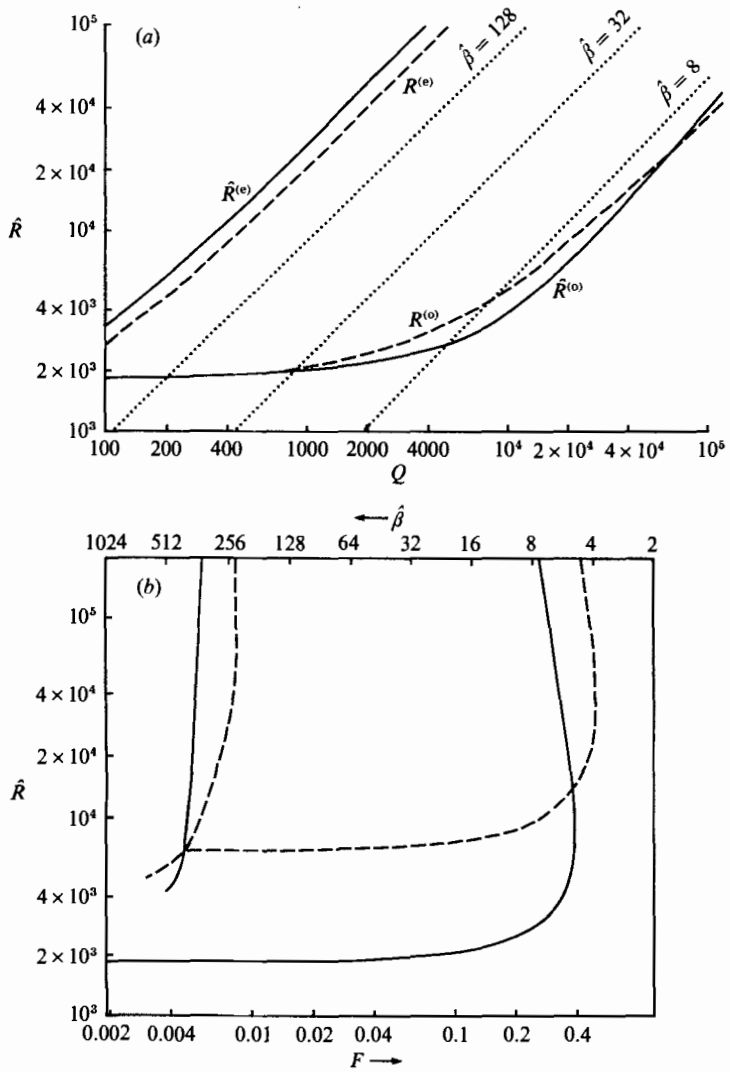

FIGURE 1. (*a*) Bifurcations from the static state ($m = 0.25$, $\chi = 1.63$, $\lambda = 2$, $\zeta = \sigma = 0.1$). The two full curves show the Rayleigh number $\hat{R}^{(e)}$ at the stationary bifurcation and the Rayleigh number $\hat{R}^{(o)}$ at the oscillatory bifurcation as functions of the Chandrasekhar number Q. The two broken curves denote the corresponding values, $R^{(e)}$ and $R^{(o)}$, in the Boussinesq limit. The dotted diagonal lines indicate constant values of F, corresponding to $\hat{\beta} = 8, 32, 128$. (*b*) Bifurcations from the static state for different aspect ratios. The full curves show $\hat{R}^{(e)}$ and $\hat{R}^{(o)}$ for $\lambda = 2$ as functions of F (on the lower axis) or $\hat{\beta}$ (on the upper axis). The broken curves show $\hat{R}^{(e)}$ and $\hat{R}^{(o)}$ for $\lambda = 1$.

For our choice of parameters

$$F = \left(\frac{3}{16\sqrt{2}}\right)\frac{Q}{\hat{R}}, \quad \hat{\beta} = \left(\frac{128}{9}\right)\frac{\hat{R}}{Q}, \quad \hat{\Phi} = \left(\frac{3}{8}\right)\left(\frac{3Q}{5\hat{R}}\right)^{\frac{1}{2}}, \tag{3.4}$$

from (2.25) and (2.26). In figure 1(*a*) we show lines of constant $\hat{\beta}$: as expected $\hat{\beta}$ decreases (and F increases) when Q is increased for constant $\hat{R}$, but F also increases if $\hat{R}$ is decreased while Q is held constant. In the Boussinesq limit we can use (3.2) to

predict the value of $R^{(o)}$ for large Q. If this value is fed into (3.3) we find that F tends to a constant value $F^{(o)}$ at $\hat{R} = R^{(o)}$ as $Q \to \infty$ and that

$$F^{(o)} = (m+1)\left\{1 - \frac{\gamma - 1}{\gamma}(m+1)\right\} \frac{4(1+\sigma)(z_0 + \frac{1}{2})^{m-1}}{\pi^2(\hat{\zeta}+\sigma)(4+\lambda^2) z_0^m}. \tag{3.5}$$

For our choice of parameters we find that $F^{(o)} \approx 0.38$ (corresponding to $\hat{\beta} \approx 5$). This provides an estimate of the largest value of F (lowest value of $\hat{\beta}$) that can be reached in the convective regime. From (3.5) it follows that the only way of increasing $F^{(o)}$ significantly is to decrease both $\hat{\zeta}$ and σ. In numerical experiments it is inconvenient to have diffusivities much lower than the values we have chosen. Thus we are unable to approach the regime with $\hat{\Phi} \approx 1$ where overstable oscillations can appear even in a stably stratified atmosphere, with $m > 1/(\gamma - 1)$ (Cattaneo 1984; Hughes & Proctor 1988). Further calculations are therefore needed to determine whether this curious instability develops into oscillations with significant amplitudes in the nonlinear regime.

As we have seen, the stability boundaries in figure 1 (*a*) run roughly parallel to lines of constant $\hat{\beta}$ for large $\hat{R}$. In figure 1 (*b*) we show $\hat{R}^{(e)}$ and $\hat{R}^{(o)}$ as functions of $\hat{\beta}$ (or F) for the two aspect ratios, $\lambda = 1$ and $\lambda = 2$, that will be considered in this paper. The value of $\hat{R}^{(o)}$ is always less for $\lambda = 2$ than for $\lambda = 1$; in this parameter range we therefore expect convection to set in with rolls of square cross-section as $\hat{R}$ is increased for a box with $\lambda = 2$. On the other hand, the minimum value of $\hat{\beta}$ for the onset of convection at a given value of $\hat{R}$ is typically less for $\lambda = 1$; as F is decreased for a given value of $\hat{R}$ ($\hat{R} > 1.4 \times 10^4$) oscillatory convection first sets in as rolls of width $\frac{1}{2}$ even in a box with $\lambda = 2$. Narrow rolls are favoured in a strong magnetic field, as in the Boussinesq regime. As $\hat{R}$ is further increased, we find that the Hopf bifurcation for rolls with $\lambda = \frac{1}{2}$ occurs at a higher value of F than that for $\lambda = 1$ provided $\hat{R} > 1.4 \times 10^5$. It is possible that the envelope of successive stability curves asymptotically approaches a fixed value of $\hat{\beta}$ as $\hat{R} \to \infty$ and $\lambda \to 0$.

In the Boussinesq approximation (valid only if $F \ll 1$ and the density scale height H is large) the velocity $\boldsymbol{u}$ is assumed to be solenoidal and acoustic modes are therefore filtered out. Thus fast magnetoacoustic waves are suppressed while slow magneto-acoustic waves reduce to transverse hydromagnetic waves which are coupled to convection. For a fully compressible stratified layer in the limit of small F (large $\hat{\beta}$) the fast magnetoacoustic waves become acoustic-gravity waves. Our reference atmosphere was chosen so as to minimize the side effects of the unstable stratification. For a disturbance with wavenumber k these depend on the parameter $\epsilon = (kH)^{-2}$, where $H = z/m$ (Lamb 1932; Priest 1982). Taking $k = \pi$ for the fundamental mode, we find that $\epsilon \approx \frac{1}{35}$ at the middle of our reference atmosphere ($z = \frac{2}{3}$) and $\epsilon \approx 0.46$ at the top ($z = \frac{1}{6}$). The frequency ω of this mode is approximately given by $\omega^2 = k^2 \hat{v}_S^2 \approx 11$, while the local cut-off frequency ω_c satisfies $\omega_c^2 = \gamma m(m+2)/4z \leqslant 1.4$ (Gough 1989). Thus $\omega > \omega_c$ throughout the layer and so we are justified in regarding fast magnetoacoustic waves as ordinary sound waves in this limit. Slow magnetoacoustic waves correspond to disturbances travelling along the field at the Alfvén speed and they are coupled to convection, giving rise to the oscillatory instability that we have described. As F is increased and the magnetic pressure becomes significant, fast and slow magnetoacoustic modes are coupled by the stratification and this interaction can be subtle when F is of order unity (as mentioned above). In a magnetically dominated layer, with $F \gg 1$, the fast magnetoacoustic waves become magneto-

gravity waves, travelling almost isotropically with a speed that differs only slightly from $\hat{v}_A$, while the slow magnetoacoustic waves reduce to sound waves, travelling along the field and modified by the stratification.

4. Nonlinear standing wave solutions ($\lambda = 2$)

The numerical experiments described in this paper are all for a perfect gas with $\gamma = \frac{5}{3}$ and $\hat{\zeta} = \sigma = 0.1$ (so that $0.0707 < \zeta < 0.1151$). The thermal boundary conditions and the total mass in the layer correspond to a static atmosphere with $z_0 = \frac{1}{6}$ and $m = 0.25$; thus the temperature increases by a factor $(z_0+1)/z_0 = 7$ across the layer, introducing significant non-Boussinesq effects, but there is only a modest density contrast ($\chi \approx 1.63$). From the linear results in the previous sections we might expect compressibility to be significant for $F \geqslant 8\times 10^{-2}$. The majority of our numerical simulations lie in the parameter range $10^{-2} \leqslant F \leqslant 0.3 (128 \geqslant \hat{\beta} \geqslant 6)$, with $4\times 10^3 \leqslant \hat{R} \leqslant 1.28\times 10^5$ and $5\times 10^2 \leqslant Q \leqslant 1.5\times 10^5$, for aspect ratios $\lambda = 2$ and $\lambda = 1$. Figure 2 shows most of the runs that were made, indicating the types of solution found at different points in the $(F,\hat{R})$-plane. Summaries of these results are presented in tables 2–4.

In this section we discuss oscillatory magnetoconvection with $\lambda = 2$ (corresponding to convective rolls with square cross-section). We shall compare two mildly nonlinear simulations at different values of $\hat{\beta}$ in order to illustrate the effect of increasing the magnetic pressure. The parameters are defined by reference to figure 2(*a*). For each value of $\hat{\beta}$ we determine the value $\hat{R}^{(o)}$ of the Rayleigh number at the oscillatory bifurcation; then we increase $\hat{R}$ by factors of 2, approximately, while holding β constant. Runs with $\hat{R}^{(o)}$, $2\hat{R}^{(o)}$, $4\hat{R}^{(o)}$, $8\hat{R}^{(o)}$, $16\hat{R}^{(o)}$, $32\hat{R}^{(o)}$ are labelled A, B, C, D, E, F respectively. Thus any run is specified by the value of $\hat{\beta}$ (an integer) and the appropriate letter, as in table 1 (which includes parameter values for all runs with $\lambda = 1$ and $\lambda = 2$). Note that increasing $\hat{R}$ for fixed $\hat{\beta}$ (as in figure 2) corresponds to increasing both $\hat{R}$ and Q in figure 1(*a*). Since F attains a maximum value ($F \approx 0.38$, $\hat{\beta} \approx 5$) on the curve $\hat{R} = \hat{R}^{(o)}$ in figure 2(*a*) the values of $\hat{R}/\hat{R}^{(o)}$ evaluated at fixed $\hat{\beta}$ and at fixed Q are different. For example, case 32B has $\hat{R} = 4\times 10^3$ and $Q \approx 1.8\times 10^3$, so that $\hat{R}/\hat{R}^{(o)} \approx 1.8$ at fixed Q, while case 8B has $\hat{R} = 5.4\times 10^3$ and $Q \approx 9.6\times 10^3$, so that $\hat{R}/\hat{R}^{(o)} \approx 1.4$ at fixed Q. Thus it is difficult to provide an unambiguous estimate of the degree of nonlinearity for runs at different values of $\hat{\beta}$.

From the linear results discussed in the previous section we expect convection to set in at $\hat{R} = \hat{R}^{(o)}$ provided $F \geqslant 10^{-3} (\hat{\beta} \leqslant 2000)$. In the immediate neighbourhood of this (supercritical) bifurcation there exist nonlinear periodic solutions. We shall first explore the range of $\hat{\beta}$ over which stable oscillatory (standing wave) solutions can be found when $\hat{R} = 2\hat{R}^{(o)}$ and then discuss two solutions in more detail. Table 2 lists the properties of stable periodic solutions for cases 6B, 8B, 32B and 128B. The period τ increases as $\hat{\beta}$ is decreased and its variation is roughly consistent with a relationship of the form $\tau = 2/v_A \approx 2/\hat{\Phi}$ that would hold for undamped hydromagnetic waves in the Boussinesq approximation. Thus the oscillatory solutions can be regarded as slow magnetoacoustic standing waves, whose global properties are only slightly modified by compressibility. The obvious global measure of superadiabatic heat transport is the Nusselt number

$$N = \left[\bar{K}^{-1}F_T - \left(\frac{dT}{dz}\right)_a\right] \Big/ \left[1 - \left(\frac{dT}{dz}\right)_a\right] \tag{4.1}$$

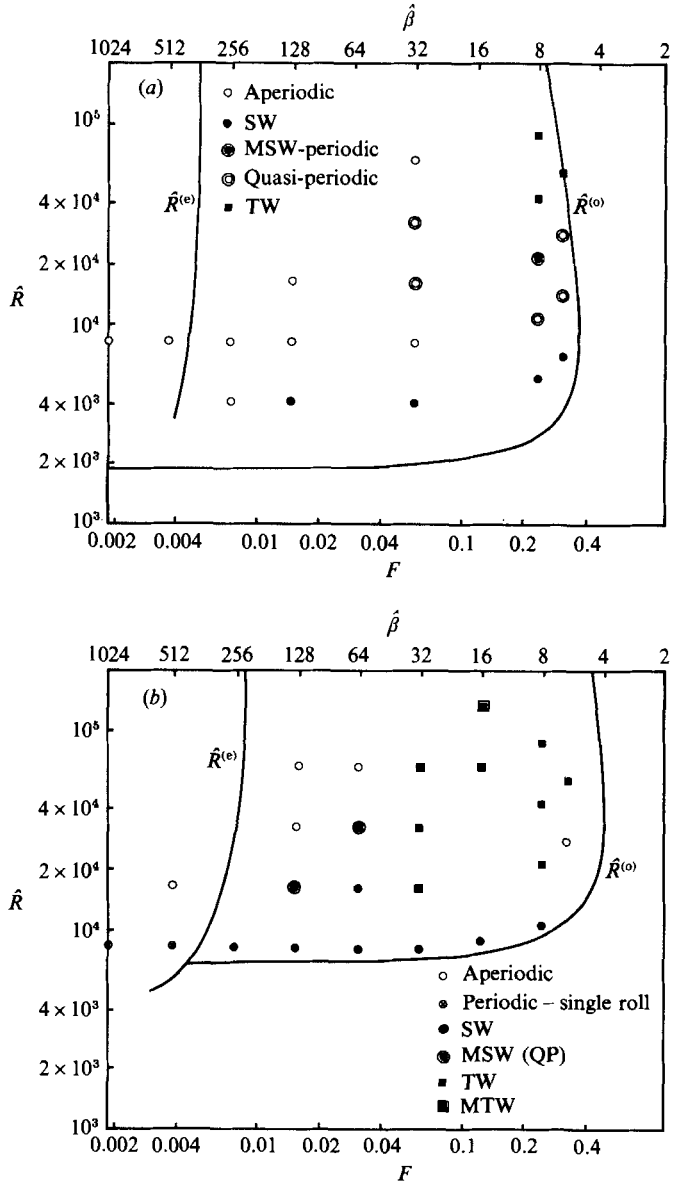

FIGURE 2. Location of solutions in the $(F,\hat{R})$-plane. (*a*) $\lambda = 2$: the curves show $\hat{R}^{(o)}$ and $\hat{R}^{(e)}$ as functions of F (on the lower axis) or $\hat{\beta}$ (on the upper axis). Nonlinear solutions are denoted by circles (standing waves) or squares (travelling waves) and hollow symbols indicate modulated solutions. (*b*) As (*a*), but for $\lambda = 1$.

evaluated at $z = 1$; here F_T is the total energy flux (cf. Hurlburt *et al.* 1984) and the dimensionless adiabatic gradient $(\mathrm{d}T/\mathrm{d}z)_a = (m+1)(\gamma-1)/\gamma$, so that $(\mathrm{d}T/\mathrm{d}z)_a = \frac{1}{2}$ for the reference atmosphere in this paper. During an oscillation the Nusselt number varies over the range $N_{\min} \leqslant N \leqslant N_{\max}$. The values of $N_{\max}$ are given in table 2 and $N_{\min} \approx 1$ for all the solutions except case 6B (where $N_{\min} \approx 0.8$). The total kinetic energy E varies over the range $0 < E \leqslant E_{\max}$ and $E_{\max}$ is greatest for case 8B. The

$\hat{\beta}$	F	$\hat{\Phi}$	$\hat{R}^{(o)} \times 10^3$ A	Values of $\hat{R}(\times 10^3)$ for cases run B	C	D	E	F	G
6	0.3143	0.4472	3.50	7.0	14.0	28.0	56.0	—	—
8	0.2357	0.3873	2.77	5.4	10.8	21.6	43.2	86.4	—
16	0.1179	0.2739	2.20	—	8.8	—	—	70.4	140.08
32	0.0589	0.1936	2.02	4.0	8.0	16.0	32.0	64.0	—
64	0.0295	0.1369	1.93	—	8.0	16.0	32.0	64.0	—
128	0.0147	0.0968	1.90	4.0	8.0	16.0	32.0	64.0	—
256	0.0074	0.0685	1.90	4.0	8.0	16.0	—	—	—

TABLE 1. Rayleigh numbers for runs in the oscillatory regime with $\lambda = 1$ or $\lambda = 2$. For each series of runs with fixed $\hat{\beta}$ (or F) the value of $\hat{R}$ is successively doubled, starting close to the value (labelled A) of $\hat{R}^{(o)}$ for $\lambda = 2$. These values can be used to calculate $Q = (128\hat{R})/(9\hat{\beta})$.

Case	τ	$N_{\max}$	$E_{\max}$	$M_{\max}$	$P_{\mathrm{m,max}}$	$\rho_{\min}$
6B	5.04	1.36	0.039	0.42	0.37	0.42
8B	5.50	1.35	0.09	0.58	0.53	0.24
32B	10.5	1.43	0.074	0.30	0.45	0.47
128B	25.0	1.16	0.025	0.13	0.20	0.72

TABLE 2. Unmodulated standing wave solutions with $\lambda = 2$

table also lists the highest local values $M_{\max}$ and $P_{\mathrm{m,max}}$ of the Mach number based on the vertical velocity

$$M = |w|/(\gamma T)^{\frac{1}{2}} \tag{4.2}$$

and of the magnetic pressure

$$P_{\mathrm{m}} = \tfrac{1}{2}F|\boldsymbol{B}|^2 \tag{4.3}$$

during an oscillation, together with the lowest local value $\rho_{\min}$ of the density. The effects of compressibility are most significant in case 8B and deviations from Boussinesq behaviour have become relatively unimportant for $\hat{\beta} = 128$.

When $\hat{\beta} = 256$ convection still sets in at a Hopf bifurcation. Case 256B showed transient oscillatory behaviour followed by a transition to apparently steady convection with $N \approx 1.63$ and $E \approx 128$. The steady solution persisted for about 50 dimensionless time units before losing stability and was followed by aperiodically modulated oscillations with asymmetric spatial structure. From studies of Boussinesq magnetoconvection with square rolls at a fixed value of the Rayleigh number we expect to find subcritical steady convection for $\hat{\beta} < \hat{\beta}^{(e)}$, where $\hat{\beta}^{(e)} \approx 530$ is the value of $\hat{\beta}$ at the stationary bifurcation ($\hat{R}^{(e)} \approx 8000$). By analogy with Boussinesq calculations there should be a branch of unstable steady solutions bifurcating from $\hat{\beta} = \hat{\beta}^{(e)}$ which acquires stability in a saddle-node bifurcation at $\hat{\beta}_{\min} < \hat{\beta}^{(e)}$, so that there is a branch of stable steady solutions for all $\beta > \beta_{\min}$ (Proctor & Weiss 1982). The Boussinesq results imply that $\hat{\beta}_{\min}$ decreases with increasing $\hat{R}$, so that $\hat{\beta}_{\min} \approx 90, 68$ for $\hat{R} = 6300, 10000$ respectively, and suggest that $\hat{\beta}_{\min}$ tends to a limit ($\hat{\beta}_{\min} \approx 30$) as $\hat{R} \to \infty$ (Weiss 1981*b*). The branch of oscillatory solutions that emerges from the Hopf bifurcation terminates in a heteroclinic bifurcation on the lower (unstable) portion of the steady branch. The behaviour of oscillatory solutions

as $\hat{R}$ is increased for fixed $\hat{\beta}$ should therefore depend on the value of $\hat{\beta}$: for $\hat{\beta}$ sufficiently small the oscillatory branch will persist for all $\hat{R}$ while for $530 \gtrsim \hat{\beta} \gtrsim 30$ the oscillatory branch will end in a heteroclinic bifurcation and there will be a transition from time-dependent to steady behaviour. The result for case 256B indicates that for $\hat{\beta} = 256$ the heteroclinic bifurcation occurs in the range $1900 < \hat{R} < 4000$ and that the upper branch of steady solutions exists but is unstable to perturbations that were suppressed in the Boussinesq approximation. Aperiodic, spatially modulated behaviour was also found in cases 256C, 128C and 128E as well as for $\hat{\beta} > \hat{\beta}^{(e)}$; it will be discussed in Part 2.

We shall compare the two cases 32B and 8B, with $F = 0.0589$ and $F = 0.2357$ respectively; we expect solutions to resemble those obtained for Boussinesq magnetoconvection in the former case while the effects of compressibility are apparent in the latter. Figure 3(*a–e*) (plate 1) and figure 4(*a–c*) (plate 2) display standing wave solutions for these two cases at equally spaced instants in time. Since the oscillations are controlled primarily by the magnetic field their frequencies are roughly proportional to the Alfvén speed and so the time spanned by a complete oscillation in figure 3 is roughly four times that for half an oscillation in figure 4. In the left-hand panels of figures 3 and 4 the velocity field is represented by randomly placed arrows or streaklines. The length of an arrow is proportional to the local speed and its direction is everywhere parallel to the instantaneous velocity; the arrows are scaled by the same factor in all frames. The colour background indicates the associated temperature fluctuation

$$T'(x, z, t) = T(x, z, t) - z \tag{4.4}$$

so that the underlying thermal stratification is suppressed. The colour coding follows the spectrum and is such that blue and violet denote numerically increasing negative values of T' while green and red denote increasing positive values of T'. The right-hand panels display lines of force of the magnetic field superimposed upon the total density in colour. We recall that the polytropic reference atmosphere has $1 \leqslant \rho(z) < 1.63$; here the range of colours from violet through blue and green to red denotes a range in density from 2 to 0 and the underlying stratification remains visible. Since the number density of field lines is proportional to the field strength, figure 4 contains twice as many field lines as figure 3.

Case 32B in figure 3 illustrates how the fluid motions wind up the magnetic field until it is strong enough to halt and then to reverse them. Thus the field provides a spring, as in the Boussinesq regime (cf. figures 6 and 7 of Weiss 1981*a*). The temperature fluctuations T' are well correlated with the vertical velocity w: hot (red) fluid rises while cold (violet) fluid sinks. The density shows three effects. First there is the underlying polytropic stratification. Secondly the density fluctuations follow the temperature fluctuations, with hotter fluid being lighter (red) than its surroundings as in the Boussinesq approximation. Thirdly there are the effects of compressibility which appear only locally and principally at the top of the layer. There the density drops dramatically in regions where the magnetic field is compressed, reaching a minimum value of 0.45, i.e. less than half the unperturbed value of $\rho(z_0)$. This is a consequence of the large magnetic pressure produced within the concentrated flux sheet. Although the magnetic pressure ($\frac{1}{2}F$) associated with the average field strength is small compared with the gas pressure P in (2.15), concentration of the field by the motion generates values of P_m that are comparable with P. This holds particularly in the upper portion of the layer, where the underlying pressure is least. Where the field is strong the gas pressure P drops in order to maintain a local magneto-

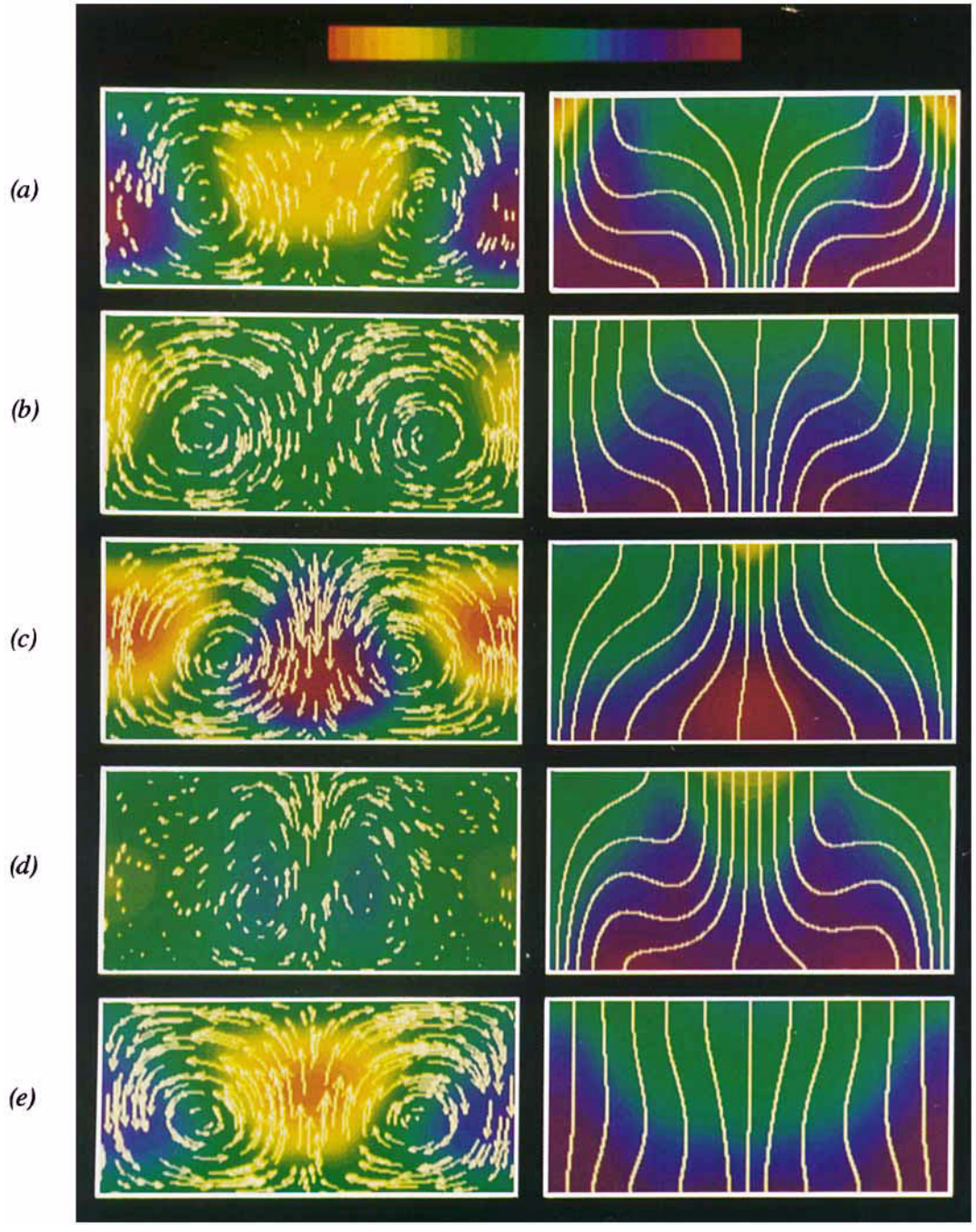

FIGURE 3. Nonlinear oscillatory magnetoconvection for an almost Boussinesq system with $\hat{\beta} = 32$ and $\hat{R} = 2\hat{R}^{(o)}$ (case 32B). The left panels show the spatial structure of the velocity streaklines and the temperature fluctuations $T'(x,z,t)$ at five almost equally spaced instants during a complete oscillation; the right-hand panels show the corresponding magnetic field lines and the total density $\rho(x,z,t)$. Cold, heavy fluid is shown at the violet end of the spectrum and hot, light fluid at the red end. The relative times are *(a)* $t/\tau = 0$, *(b)* $t/\tau = 0.196$, *(c)* $t/\tau = 0.397$, *(d)* $t/\tau = 0.597$, *(e)* $t/\tau = 0.798$, where the period $\tau = 10.19$.

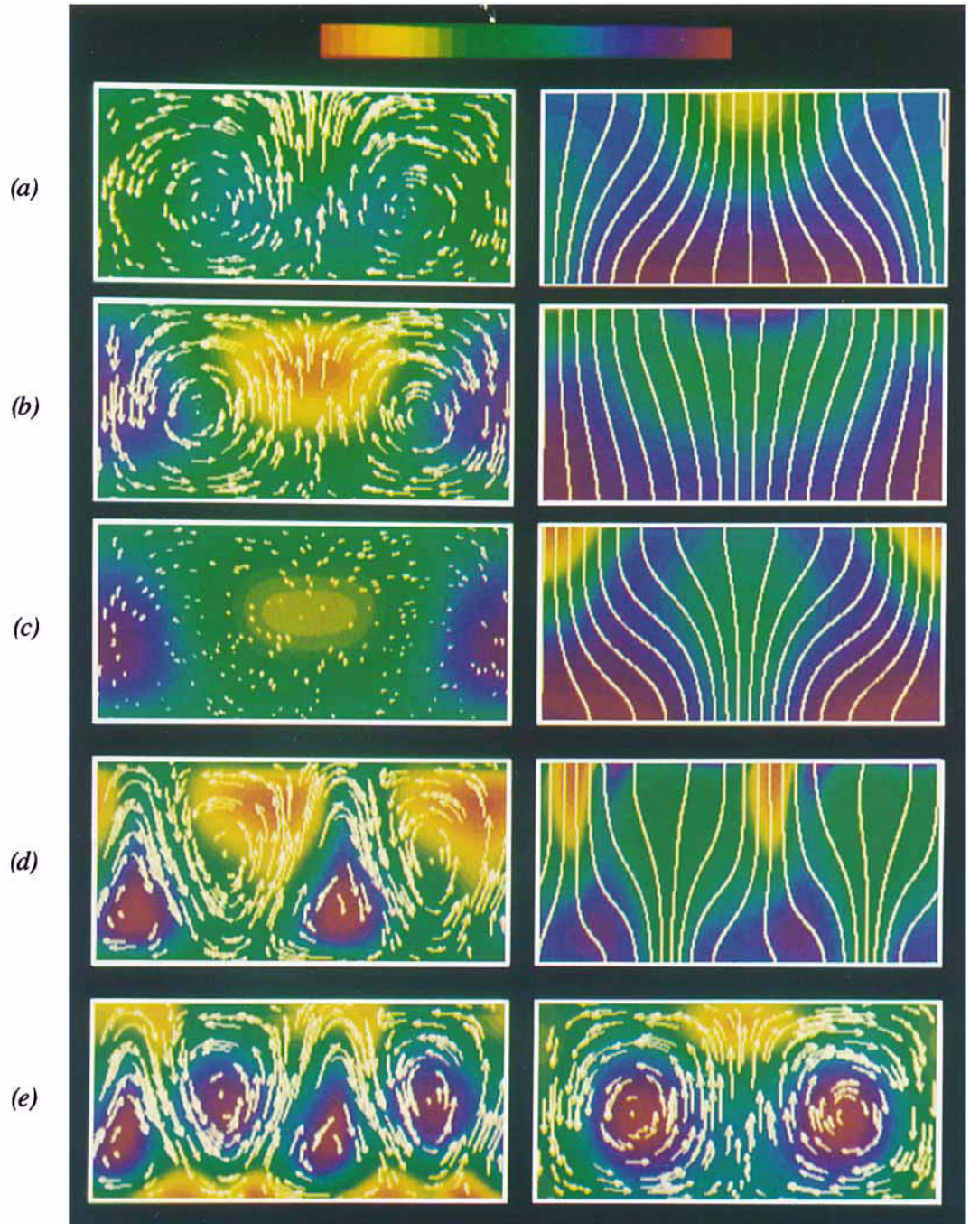

FIGURE 4. Standing waves in a compressible layer with $\hat{\beta} = 8$ and $\hat{R} = 2\hat{R}^{(o)}$ (case 8B): streaklines, temperature fluctuations, field lines and density over half a complete oscillation, at times *(a)* $t/\tau = 0$, *(b)* $t/\tau = 0.211$, *(c)* $t/\tau = 0.422$, where the period $\tau = 4.81$. *(d)* The same, but for a travelling wave solution with $\hat{\beta} = 8$ and $\hat{R} = 16\hat{R}^{(o)}$ (case 8E). *(e)* Velocity streaklines and fluctuations in total pressure $\Pi(x,z,t)$ for the travelling wave solution (case 8E) in the left panel and the standing wave solution (case 8B) in the right panel; low pressure is shown at the violet end of the spectrum and high pressure at the red end.

hydrostatic equilibrium (cf. Hurlburt & Toomre 1988) and the consequent reduction of density is achieved by partial evacuation of the flux sheet. The decreased density in turn leads to a buoyancy force which opposes the descending motion in regions where the field is swept together by a horizontally converging flow. Later, as the velocity reverses, the buoyancy accelerates the ascending fluid. Because the local region of magnetic buoyancy tends to generate motion on its own scale the reversal first appears as a narrow convective plume within the flux sheet, as seen at $t \approx 0.6\tau$ in figure 3(*d*). Note that magnetic buoyancy assists upward motion at the lower boundary and resists downward motion at the upper boundary, where it is more effective. Thus the main dynamical consequence of compressibility is that magnetic buoyancy produces short bursts of upwelling into the flux sheets as the flow reverses. These vigorous spurts have no analogue in the fully Boussinesq regime.

When the field strength is doubled the oscillations assume a different form. The magnetic field for case 8B, in figure 4, is relatively less distorted than in figure 3. On the other hand, magnetic buoyancy is more potent. The velocity and temperature appear similar in cases 8B and 32B, although smaller-scale motions (with corresponding temperature fluctuations) are no longer evident in the former case. However, the density fluctuations (and hence the buoyancy forces) are now controlled by variations in magnetic pressure rather than by changes in temperature. Moreover, variations in $|\boldsymbol{B}|$ and T' have the same horizontal scale in figure 4 and so magnetic buoyancy drives large-scale motion, rather than the local spurts of figure 3(*d*). When the field lines are only slightly distorted, as in figure 4(*b*), the density is mainly determined by the temperature, so motion is driven by thermal buoyancy. As the field is modified magnetic buoyancy takes over. In figure 4(*a*) thermally induced variations in density can still be detected but the predominant effect is a reduction in ρ where P_m is large and a corresponding increase where P_m is small. At the base of the layer thermal and magnetic buoyancy act together; at the top they are opposed. Since that is where magnetic buoyancy is most powerful, the net effect of compressibility is that the magnetic pressure assists magnetic tension (which provides the spring) in opposing any motion. Hence the oscillations have a short period and low amplitude.

In order to contrast detailed properties of these oscillatory solutions we display several time series in figure 5(*a*) and (*b*) for cases 32B and 8B respectively. Successive rows show the variation with time of the kinetic energy E (which is almost sinusoidal), the minimum value of the density $\rho_{\min}$, the peak value of the magnetic field expressed as an Alfvén speed

$$B_{\max} = F^{\frac{1}{2}}\bar{B} = (\mu_0 R_* \rho_0 \Delta T)^{\frac{1}{2}}\bar{B}, \tag{4.5}$$

where $\bar{B}$ is the maximum value of $|\boldsymbol{B}|$ (cf. (2.15) and (2.16)), the peak value $M_{\max}$ of the Mach number based on the vertical velocity, and the Nusselt number N evaluated at $z = 1$.

$B_{\max}$ for $\hat{\beta} = 32$, displayed in figure 5(*a*), shows a nearly sinusoidal variation with a period $\tau = 10.5$, about twice the Alfvénic transit time. At its peak the magnetic field at the base of the layer is amplified almost fourfold over its average value. The minimum density follows the maximum field with some significant deviations. At times of small field amplification $\rho_{\min}$ changes slowly but near maximal amplification it varies rapidly; $\rho_{\min}$ reaches its minimum value shortly before $B_{\max}$ attains its peak and then increases to more moderate values. Both $M_{\max}$ and N possess more structure: $M_{\max}$ rises rapidly to 0.30 as the field begins to relax towards a less concentrated state and then levels off, while $B_{\max}$ is a minimum before dropping to

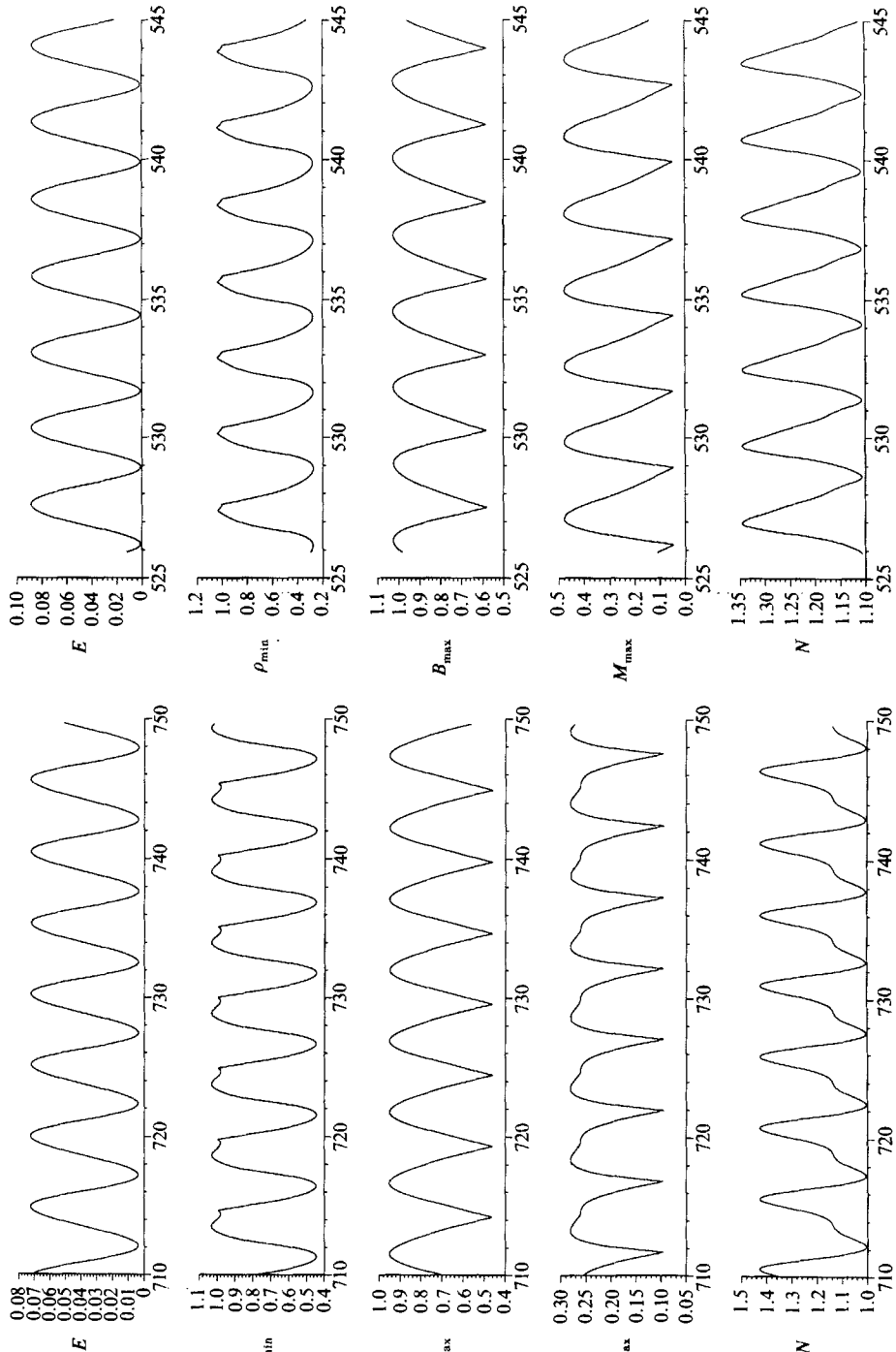

FIGURE 5. Time-dependent behaviour for standing wave solutions ($\lambda = 2$). (*a*) Case 32B: variation with time of the kinetic energy E, the minimum value ρ_{min} of the density, the maximum value B_{max} of the normalized magnetic field, the maximum value M_{max} of the Mach number and the Nusselt number N. (*b*) As (*a*) but for case 8B.

0.12 as $B_{\max}$ increases once more. The jagged peak in $M_{\max}$ is caused by magnetic buoyancy within the flux sheets, which provides an impulse as the field begins to unwind; the resulting motion fills the flux sheets and eliminates the extra buoyancy. Thus a flux sheet is only evacuated for part of its lifetime. Note that the rapid rise in the vertical velocity is a consequence of density changes caused by pressure fluctuations. This effect is excluded in Boussinesq magnetoconvection where the velocity typically reaches a peak when $B_{\max}$ is a minimum (Weiss 1981*a*). However, N reaches its peak just as $M_{\max}$ approaches its minimum and $B_{\max}$ is beginning to increase. This confirms the impression from figure 3 that the strong rising flow caused by magnetic buoyancy within the flux sheet is only a local phenomenon. Indeed, other global properties of this solution (e.g. the kinetic energy) behave much as in the Boussinesq limit despite the difference in the detailed structure of the motion.

When $\hat{\beta} = 8$ the period $\tau = 5.49$, suggesting that $\tau \propto B_0^{-1}$ although the two solutions are very different. The variation of $B_{\max}$, in figure 5(*b*), shows a slight asymmetry, with the rise time longer than the decay time. The peak value is slightly greater than that for $\hat{\beta} = 32$ but only corresponds to a doubling of the average field strength. The minimum density also shows a slight asymmetry and follows $B_{\max}$ more closely than in the previous example (though $\rho_{\min}$ precedes $B_{\max}$ by a small phase shift). The lowest value of $\rho_{\min}$ is about one quarter of the mean density, indicating a greater degree of evacuation than before. $M_{\max}$ attains a higher peak of 0.59 and both $M_{\max}$ and N exhibit more regular variation. The peak value N is only 1.35; the degree of field concentration, the maximum field strength and the Nusselt number all decrease with increasing F. Finally we note that the slight asymmetries in the variations of $B_{\max}$, $M_{\max}$ and $\rho_{\min}$, as well as differences in phase, are necessary in order to extract energy from magnetic buoyancy forces.

5. Travelling waves in magnetoconvection

When convection first appears at a Hopf bifurcation the complex eigenfunctions at the bifurcation point have the form $u = U(z)\exp \mathrm{i}(ax \pm \omega t)$ etc., where a is the horizontal wavenumber of the perturbation. In an infinite layer these solutions correspond to travelling waves, with $u \propto \sin(ax \pm \omega t)$, or to a standing wave, with $u \propto \sin ax \cos \omega t$ (for a suitably chosen origin in the (x, t)-plane). In a finite region of width λ the fundamental mode has $a = 2\pi/\lambda$ and the allowable solutions depend on the choice of lateral boundary conditions. If the horizontal velocity $u = 0$ at $x = 0$, λ (as in most Boussinesq calculations), then only standing waves are allowed; if periodic boundary conditions are imposed then both travelling wave and standing wave solutions are permitted. Thus two branches of time-dependent solutions emerge from the same Hopf bifurcation at $\hat{R} = \hat{R}^{(0)}$ and nonlinear effects determine which branch is preferred. For example, laboratory experiments on convection in a rotating system show oscillatory behaviour, corresponding to standing waves (Rossby 1969) while travelling waves have been observed for convection in a two-component (ethanol–water) mixture (e.g. Walden *et al.* 1985). In numerical experiments on two-dimensional thermosolutal convection travelling waves were first detected by D. R. Moore (private communication) and have since been investigated in considerable detail (Knobloch *et al.* 1986; Deane, Knobloch & Toomre 1987).

The results presented in §4 show that standing wave solutions with $\hat{R} = 2\hat{R}^{(0)}$ are stable for $\lambda = 2$. If, however, we take case 8B in figure 4 and increase the Rayleigh number by a factor eight while holding F fixed then the standing waves evolve into

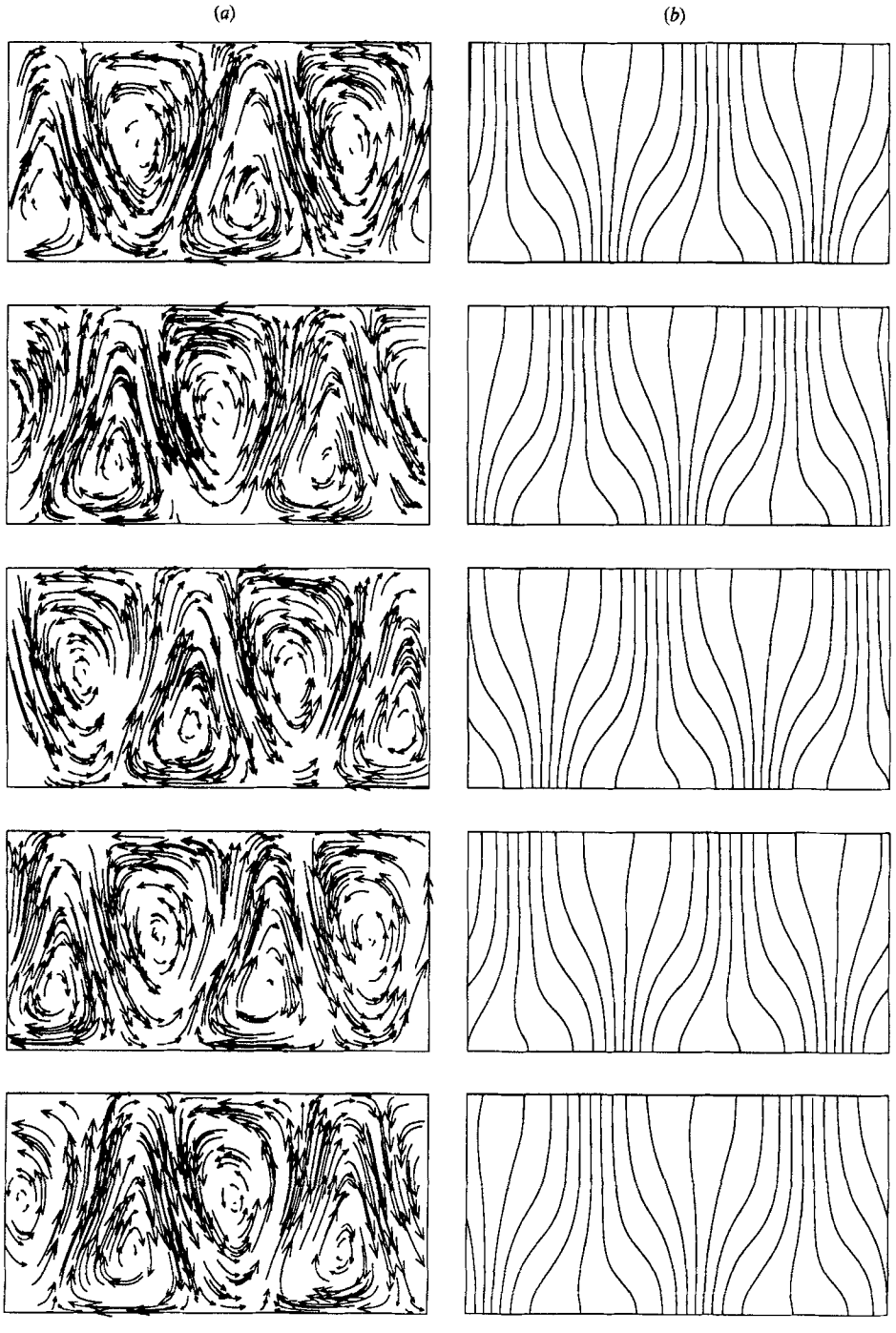

FIGURE 6. Travelling waves with $F \approx 0.24$ and $\hat{R} = 16R^{(0)}$ (case 8E). (*a*) Velocity streaklines and (*b*) magnetic field lines at equally spaced instants in time, separated by a time interval $\delta t \approx 1.9$. The wave pattern propagates with a speed $v = 0.126$ towards the right.

stable travelling waves. Figure 6 shows the velocity and magnetic field for case 8E ($\hat{R} = 43200, Q = 38400$) at five equally spaced instants in time. There are now four rolls in the computational domain and the pattern is translated at a uniform velocity from left to right. Each roll is roughly triangular in cross-section and the rolls with a clockwise sense of motion point upwards while those with anticlockwise motion point downwards. (There is an equivalent solution with the rolls oppositely oriented and the wave travelling to the left.) Rising fluid no longer moves vertically. Instead, a continuous jet of fluid zigzags from top to bottom of the layer along the peripheries of the triangular rolls. Within this jet the horizontal velocity is in the same direction as the wave velocity. Since there is no net momentum in the system the mass flux in the jet is balanced by oppositely directed motion elsewhere in the layer. The magnetic field is compressed at the narrower vertices of the rolls but is much weaker at their bases. In the interior of the layer the field direction is more or less parallel to the jet though the boundary conditions ensure that $\boldsymbol{u}$ and $\boldsymbol{B}$ are perpendicular at $z = z_0, z_0 + 1$. Since the pattern remains steady in a reference frame moving with the wave velocity all global measures of the solution are invariant in time. Here $N \approx 2.4$, while $P_{\mathrm{m,max}} \approx 0.8$, $M_{\max} \approx 0.45$, $\rho_{\min} \approx 0.35$ so the solution is far from the Boussinesq regime.

Figure 4(*d*) shows the relationship between velocity and temperature fluctuations (on the left) and magnetic field and total density (on the right) for this travelling wave solution. Comparison with figure 4(*a–c*) shows that the mirror symmetry about planes separating adjacent rolls, which is present in the standing wave solution, is broken in the travelling wave solution. (Note, however, that the Lagrangian trajectories of individual fluid elements still conform to a roughly rectangular pattern as the triangular waves pass by. In contrast, travelling waves in thermosolutal convection have rolls with trapezoidal cross-sections which become more marked if individual trajectories are followed.) This loss of symmetry in the nonlinear regime is associated with the distinction between positive and negative wave velocities. It is shown most clearly by the prograde velocity in the jet.

The temperature fluctuations are produced by the convective motion. For the standing wave solution, symmetry requires that the temperature and velocity should maintain the same phase in x, though the temperature lags in time. In the travelling wave solution the temperature lags behind the velocity pattern as it moves. The density fluctuations in figure 4(*d*) are centred on regions of strong field at the upper and lower boundaries, confirming that the flux sheets are partially evacuated. Once again the density distribution reflects variations of pressure rather than variations of temperature.

Pressure variations are important in the dynamics of these travelling waves. Figure 4(*e*) shows, on the left, streaklines for the travelling wave solution in figure 6 superimposed on the fluctuations in total pressure,

$$\Pi'(x, z, t) = P + \tfrac{1}{2}F|\boldsymbol{B}|^2 - (z^{m+1}/z_0^m). \tag{5.1}$$

The horizontally averaged values of Π' are negative in the interior of the layer and positive at the boundaries while minima are located at the centres of the rolls. For fixed z, Π' is a maximum ($\partial\Pi'/\partial x = 0$) on the jet. This contrasts with the behaviour of standing wave solutions, as illustrated on the right in figure 4(*e*). The relation between pressure and velocity varies during an oscillation but the illustration shows a typical pattern for case 8B. Here the pressure maxima are aligned with rising and falling plumes, with clear minima where the horizontal speed is greatest.

In case 8E the waves travel with a velocity $v \approx 0.215$. At the centre of the layer

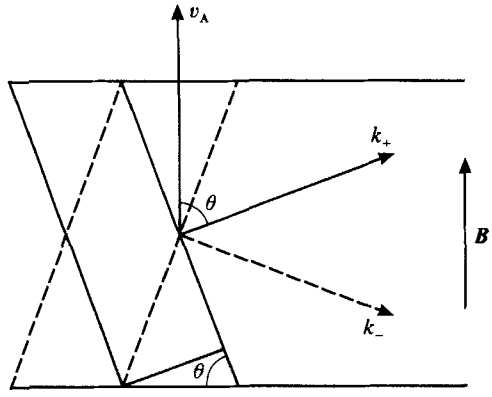

FIGURE 7. Slow magnetoacoustic waves in the Boussinesq approximation. Sketch illustrating the relationship between the group velocity (parallel to the magnetic field $\boldsymbol{B}$), the phase velocity v_P of plane waves travelling at an angle θ to the field and the velocity v of travelling waves produced by interference between waves travelling in directions $\theta, \pi-\theta$ to $\boldsymbol{B}$.

the sound speed $\hat{v}_S \approx 1.05$ and the Alfvén speed $\hat{v}_A \approx 0.41$. We recall that in an unstratified medium with a uniform vertical magnetic field such that $\Phi = v_A/v_S < 1$ pure Alfvén waves and slow magnetoacoustic waves can travel vertically at the Alfvén speed while fast magnetoacoustic waves can travel horizontally with a phase velocity $v = (v_S^2 + v_A^2)^{\frac{1}{2}}$. Fast waves travelling in the x-direction would be unaffected by horizontal boundaries; motion would be purely longitudinal and driven by the enhancement (reduction) of total pressure at condensations (rarefactions). The actual wave speed is, however, significantly less than the sound speed so the travelling waves are not examples of fast magnetoacoustic waves.

For $\Phi \ll 1$ the slow magnetoacoustic waves reduce to transverse hydromagnetic waves, representing disturbances that travel along the field at the Alfvén speed. In the Boussinesq limit undamped plane hydromagnetic waves travelling at an angle θ to the vertical magnetic field have a phase velocity $v_P = v_A \cos\theta$. Such waves will be reflected at a horizontal plane and a configuration with boundaries at $z = z_0, z_0 + 1$ therefore acts as a waveguide. Two waves of equal amplitude, travelling at angles θ, $\pi - \theta$ to the vertical with wave vectors $\pi(\tan\theta, 0, \pm 1)$ can be combined to produce a travelling wave with horizontal wavelength $\lambda = 2\cot\theta$, as indicated in figure 7. Then the wave travels with the speed of the wavefronts, so

$$v = v_P/\sin\theta = v_A \cot\theta = \tfrac{1}{2}\lambda v_A. \tag{5.2}$$

Although isolated disturbances only travel along the magnetic field the boundary conditions allow horizontally propagating waves. Moreover the four-roll solutions that we have found correspond to waves with $\lambda = 1$ and $v = \frac{1}{2}v_A$. In our case the waves travel with a velocity $v \approx 0.53\hat{v}_A$, suggesting that they are essentially slow magnetoacoustic waves and still adequately described within the Boussinesq approximation. (The relevant small parameter is really $\hat{\Phi}^2 \approx 0.15$.)

Nevertheless, the correspondence between $\boldsymbol{u}$ and Π' in figure 4(*e*) shows the pressure fluctuations are important in the nonlinear regime. For waves driven by fluctuations in total pressure only, the horizontal component of the equation of motion takes the form

$$\rho \frac{\partial}{\partial t}[u(x-vt, z)] = -\frac{\partial}{\partial x}[\Pi'(x-vt, z)]. \tag{5.3}$$

Hence it follows that $\Pi' = \rho v u$. In particular, for fixed z the maxima of the pressure fluctuations and the prograde velocity must coincide. This clearly holds for figure 4(*e*), where Π' is high on the jet. We note, moreover, that since the pressure fluctuation Π' is a maximum at stagnation points on the upper and lower boundaries Π' would attain a minimum where $|u|$ was a maximum for rolls with rectangular cross-section. With a triangular cross-section it is possible for both Π' and the prograde velocity to be maximal at the vertices. The appearance of triangular rolls and the associated jet can therefore be explained if pressure fluctuations are locally more important than curvature forces in the equation of motion.

Our discussion of travelling waves has so far been related only to the solutions illustrated in figures 6 and 7, for case 8E. Similar waves are found when the Rayleigh number is doubled (case 8F) and also when F is increased from 0.24 to 0.31 (case 6E). We did not, however, find travelling wave solutions for runs with $\lambda = 2$ and $F \approx 0.06$ ($\hat{\beta} = 32$). These results all suggest that the travelling waves are a 'low β' phenomenon; when $\hat{\beta} = 6$ the magnetic pressure is almost equal to the thermal pressure at the upper boundary. Since they only appear with rolls of width 0.5 the interaction between standing wave and travelling wave solutions is best explored in a narrower domain with $\lambda = 1$.

6. Transition from standing waves to travelling waves ($\lambda = 1$)

In systems where convection sets in through an oscillatory (or Hopf) bifurcation the first question to be answered is whether standing waves or travelling waves are preferred in the neighbourhood of the Hopf bifurcation. The two-dimensional problem is periodic in x and symmetric with respect to lateral translations and to reflection in a vertical plane. These are symmetries of the orthogonal group $O(2)$ and the Hopf bifurcation with $O(2)$ symmetry is discussed by Golubitsky & Stewart (1985) and Stewart (1988). The bifurcating solutions have spatial symmetries corresponding to the groups $SO(2)$ and Z_2 for travelling waves and standing waves respectively. Provided that both solution branches bifurcate supercritically, the branch with greater r.m.s. amplitude (averaged over space and time) is stable and that with lesser amplitude is unstable (Ruelle 1973; Golubitsky & Stewart 1985; Knobloch *et al.* 1986). In the case of thermosolutal convection, where the amplitude equations are degenerate, travelling waves are always preferred (Bretherton & Spiegel 1983; Knobloch *et al.* 1986; Deane *et al.* 1987).

If the evolution equations are extended by including higher-order terms it becomes possible to describe secondary bifurcations, giving rise to branches of mixed-mode (or modulated wave) solutions that allow a transfer of stability from standing waves to travelling wave or vice versa (Deane *et al.* 1987). Dangelmayr & Knobloch (1987) have carried through a more ambitious programme: they analyse the relationship between standing wave, travelling wave, modulated wave and steady solution branches by unfolding the degenerate (codimension-two) Bogdanov bifurcation with $O(2)$ symmetry and assemble thirty allowable bifurcation diagrams.

Although there has been no systematic search for travelling waves in Boussinesq magnetoconvection, behaviour in the neighbourhood of the oscillatory bifurcation has been studied for rolls with different aspect ratios. For $Q \gg 1$, it follows from (3.2) that $R^{(0)}$ is a minimum for narrow rolls, with $\lambda \sim Q^{-\frac{1}{6}}$; in that limit, travelling waves are apparently preferred (Proctor 1986). As $R^{(0)}$ is increased *wider rolls rapidly* become unstable. A discussion of the codimension-two bifurcation for $\lambda = 2\sqrt{2}$, in the limit $\sigma, \zeta \to 0$, indicates that standing waves are preferred (Nagata 1986;

Case	τ	$N_{\max}$	$E_{\max}$	$M_{\max}$	$P_{m,\max}$	$\rho_{\min}$
8C	5.4	1.18	0.007	0.21	0.27	0.70
(8D)	5.3	2.29	0.032	0.50	0.56	0.34
16C	7.2	1.08	0.007	0.18	0.20	0.77
32C	9.9	1.07	0.004	0.13	0.11	0.87
(32D)	8.8	1.98	0.035	0.37	0.50	0.53
64C	14.0	1.07	0.004	0.12	0.08	0.89
64D	12.1	1.69	0.028	0.29	0.39	0.59
128C	21	1.06	0.003	0.12	0.05	0.92
128D	12.2	1.69	0.028	0.29	0.40	0.58
256C	39	1.05	0.003	0.11	0.03	0.93

TABLE 3. Unmodulated standing wave solutions with $\lambda = 1$. Brackets indicate unstable cases

Case	v	N	E	$M_{\max}$	$P_{m,\max}$	$\rho_{\min}$
6D*	0.21	1.91	0.041	0.43	0.7	0.4
6E*	0.223	2.37	0.053	0.49	0.81	0.30
(8C)	0.190	1.13	0.008	0.18	0.275	0.74
8D	0.198	1.86	0.041	0.37	0.661	0.45
8E	0.215	2.39	0.056	0.45	0.852	0.35
8F	0.215	2.71	0.061	0.52	0.92	0.28
16F	0.168	2.80	0.059	0.47	0.91	0.42
(32C)	0.101	1.03	0.002	0.08	0.076	0.92
32D	0.116	1.42	0.019	0.17	0.323	0.71
32E	0.126	1.93	0.031	0.25	0.541	0.61
32F	0.130	2.41	0.038	0.37	0.603	0.57
32F ($\sigma = 1$)	0.087	2.7	0.012	0.16	0.30	0.56

TABLE 4. Unmodulated travelling wave solutions with $\lambda = 1$. Brackets indicate unstable cases; asterisks indicate cases with $\lambda = 2$

Dangelmayr & Knobloch 1986). In what follows we shall first describe relevant numerical experiments on compressible magnetoconvection and then attempt to relate them to these theoretical results.

We have obtained solutions for $\lambda = 1$ with $\hat{\beta} = 8$, 32, 64, 128 and 256. For each value of $\hat{\beta}$ we investigate the nature of the preferred time-dependent solution by increasing $\hat{R}$ (by factors of two) starting just above the values $\hat{R}^{(o)}$ at the oscillatory bifurcation. Figure 2(*b*) indicates the runs made and the nature of the preferred solutions; further details are provided in tables 3 and 4. The branches of standing waves and travelling waves apparently emerge supercritically at $\hat{R}^{(o)}$. In the neighbourhood of the Hopf bifurcation we expect one of these branches to be stable and the other to be unstable. The growth rates of the relevant perturbations are, however, proportional to $(\hat{R}-\hat{R}^{(o)})$ and unstable solutions may survive for a long time. Certain choices of initial conditions may therefore lead to persistent transient behaviour; in particular, we find that simple perturbations to a static solution often develop into nonlinear standing waves even when travelling waves are preferred.

We consider first the runs with $\hat{\beta} = 8$, where travelling waves were found at

$\hat{R} = 4.52\hat{R}^{(o)}$ for case 8E (cf. figure 6). For case 8C ($\hat{R}/\hat{R}^{(o)} \approx 1.13$) the run, started from a perturbed static solution, developed into stable standing waves with the properties listed in table 3. Another run, started from a travelling wave solution (for case 8E), yielded an almost steady travelling wave with properties listed in table 4. A third run, started from a linear combination of the previous pair, eventually settled down to a pure standing wave solution. The same procedure was repeated for case 8D ($\hat{R}/\hat{R}^{(o)} \approx 2.26$). Again both standing waves and travelling wave solutions were obtained but the linear combination settled down to a pure travelling wave solution. Travelling waves were also found for cases 8E and 8F. As expected, the triangular cross-section of the rolls and the associated jet become more prominent as $\hat{R}$ is increased. In the unstable travelling wave solution for case 8C the cross-section deviates only slightly from a rectangle.

With $\hat{\beta} = 16$ we found a stable standing wave solution for case 16C and a stable travelling wave solution for case 16F. Case 16G (with $\hat{R}/\hat{R}^{(o)} \approx 17$) exhibited more complicated behaviour, with a modulated travelling wave solution in which N varied periodically about its mean value with an amplitude of about 6% and a modulation period $\tau_m \approx 5.25$.

Runs for $\hat{\beta} = 32$ show behaviour similar to that found for $\hat{\beta} = 8$. For case 32C ($\hat{R}/\hat{R}^{(o)} \approx 1.11$) the stable standing wave solution has $N_{max} \approx 1.07, E_{max} \approx 3.4$. Travelling waves have $N \approx 1.034, E \approx 1.61$ and show a slight periodic modulation with very slowly increasing amplitude, while a combination of the two ends up as a standing wave. For case 32D it is again possible to generate standing wave or travelling wave solutions but a combination develops into a travelling wave. Cases 32E and F also yield steady travelling waves.

With $\hat{\beta} = 64$ standing waves seem to remain stable up to $\hat{R}/\hat{R}^{(o)} \approx 2.3$ (case 64D) and a quasi-periodic modulated travelling wave appears in case 64E. The Nusselt number and the kinetic energy vary cyclically with $1.2 \leqslant N \leqslant 2.4$ and $3 \leqslant E \leqslant 35$ but are bounded away from their values for the static state. The cyclic variation has a period $\tau \approx 11.8$ and is itself modulated with a period $\tau_m \approx 44$. Although the velocity reverses its direction, there is no symmetry plane between adjacent rolls. Figure 8(*a*) shows streaklines when the kinetic energy is near a local maximum. The rolls have a slightly triangular structure, with their centres alternately displaced upward and downward (as in the travelling wave solutions). This modulated wave seems to be a 'mixed-mode' solution associated with the transition from standing wave to travelling wave solutions. When $\hat{R}$ is increased, however, no travelling waves are found. The solution for case 64F ($\hat{R}/\hat{R}^{(o)} \approx 9.1$) is aperiodically modulated and shows a greater variety of spatial structure, varying from the asymmetrical rolls in figure 8(*b*) to the almost symmetrical pattern of figure 8(*c*).

No travelling waves were found for $\hat{\beta} = 128$. At $\hat{R}/\hat{R}^{(o)} \approx 1.19$ (case 128C) runs started either by perturbing the static solution or from a travelling wave both converged on a standing wave solution with period $\tau \approx 21$. Case 128D yielded a quasi-periodic modulated wave with a cycle period $\tau \approx 19$ and a modulation period $\tau_m \approx 66$. This is apparently a mixed-mode solution of the same type as case 64E. Cases 128E and 128F both led to aperiodically modulated waves.

Finally, case 256C provided a standing wave with a longer period ($\tau \approx 39$). From figure 1(*b*) the stationary bifurcation occurs at $\hat{\beta}^{(e)} \approx 370$ for $\hat{R} = 8000$ and there is no longer an oscillatory bifurcation beyond the codimension-two bifurcation at $\hat{\beta} = 430$. Indeed, a run at $\hat{\beta} = 512, \hat{R} = 8000$ showed a solution whose amplitude grew monotonically from an initial perturbation until it saturated to give a transient steady solution which subsequently lost stability and was followed by periodic

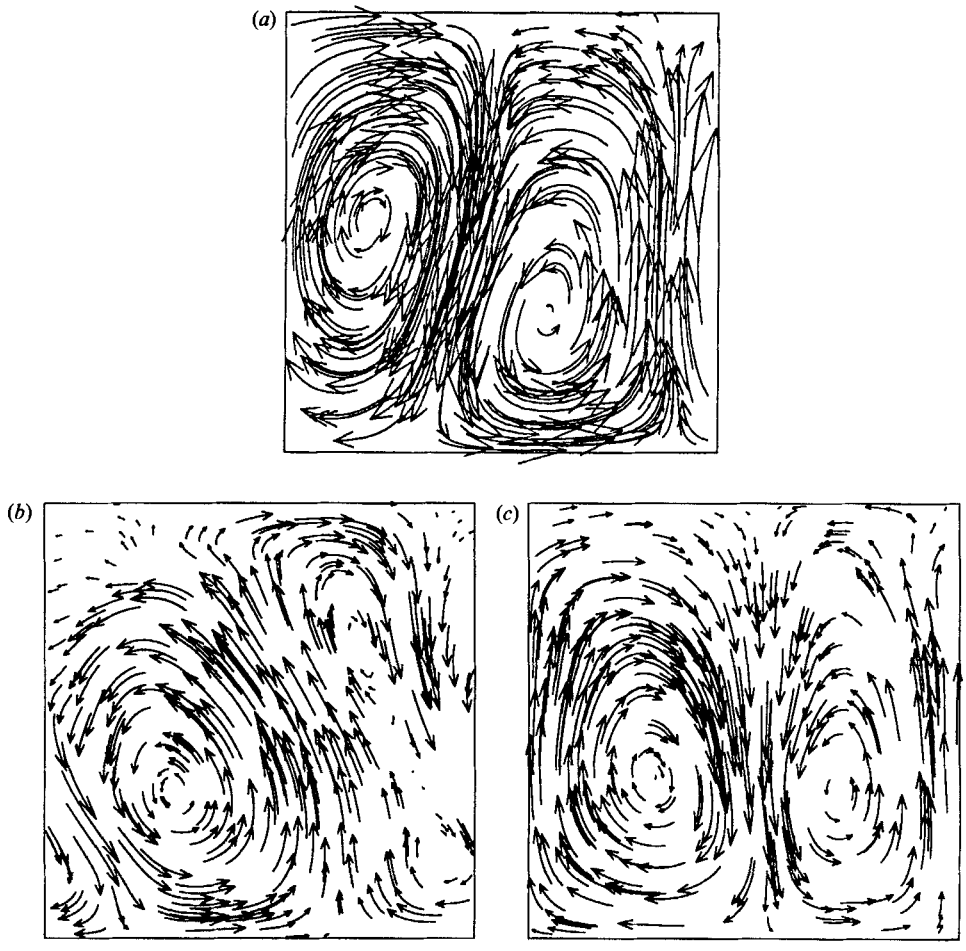

FIGURE 8. Quasi-periodic and aperiodic modulated waves ($\lambda = 1$). (*a*) Streaklines for quasi-periodic mixed-mode solution when the kinetic energy is large (case 64E). (*b*, *c*) Symmetry breaking in the aperiodic solution for case 64F.

oscillations that are qualitatively different from those described here. This behaviour (which is absent for $\hat{\beta} \leqslant 256$) will be discussed in Part 2.

From these numerical experiments it is clear that stable standing wave solutions exist for $R \approx 2R^{(o)}$ over the whole range $256 \geqslant \hat{\beta} \geqslant 8$. The period τ of these solutions is plotted logarithmically against $\hat{\beta}$ in figure 9(*a*). For $16 \leqslant \hat{\beta} \leqslant 128$ these results are roughly consistent with a relationship of the form

$$\tau = \frac{2}{v_A} \approx \frac{2}{\hat{\Phi}} (\gamma \hat{T})^{-\frac{1}{2}} = (3\hat{\beta})^{\frac{1}{2}} \tag{6.1}$$

which would hold for undamped standing waves in the Boussinesq approximation. Moreover this expression for τ is independent of the aspect ratio λ and figure 9(*a*) confirms that the periods for $\lambda = 1$ and $\lambda = 2$ differ only slightly. For $\hat{\beta} > 128$ the period τ increases more rapidly. This is to be expected since there is a codimension-two bifurcation at $\hat{\beta} \approx 430$, where $R_T^{(o)} = R_T^{(e)}$. At such a degenerate bifurcation there are two zero eigenvalues, so the period of the oscillations must become infinite. Over

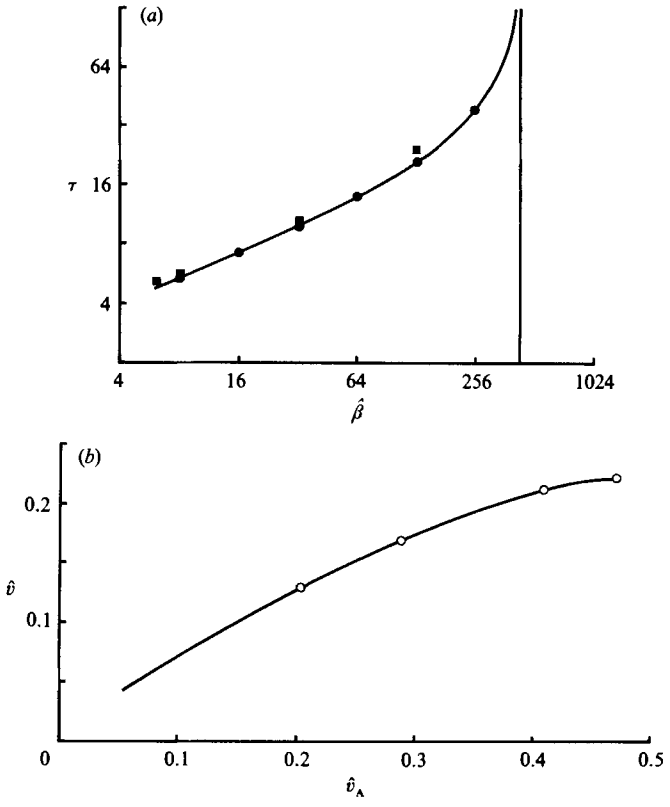

FIGURE 9. Standing waves and travelling waves ($\lambda = 1$). (*a*) Period τ of standing waves as a function of $\hat{\beta}$; circles and squares indicate results for $\lambda = 1, 2$ respectively. (*b*) Velocity $\tilde{v}$ of travelling waves as a function of the Alfvén speed $\hat{v}_A$.

the range $\hat{\beta} \geqslant 16$ the periodic oscillations are adequately described by the Boussinesq model; it is only for $\hat{\beta} \leqslant 8$ that compressional effects raise the period τ above the value given by (6.1).

In the numerical experiments travelling wave solutions were always unstable for $\hat{R}$ sufficiently close to $\hat{R}^{(0)}$. The travelling waves acquired stability as $\hat{R}$ was increased for $\hat{\beta} \leqslant 32$. We can describe such transitions by normal form equations that are generically valid in the neighbourhood of the initial bifurcation and this description will remain qualitatively correct over a finite range as the parameters are varied (Guckenheimer & Holmes 1983). In the neighbourhood of the Hopf bifurcation the interaction between weakly nonlinear travelling waves and two-roll standing waves can be modelled by the simplified normal form equations

$$\left.\begin{aligned} \dot{r}_1 &= r_1[\lambda - (r_1^2 + r_2^2) - a r_2^2 - b r_2^4], \\ \dot{r}_2 &= r_2[\lambda - (r_1^2 + r_2^2) - a r_1^2 - b r_1^4], \end{aligned}\right\} \tag{6.2}$$

where r_1, r_2 are the amplitudes of travelling waves propagating to the left and right respectively, the parameter $\lambda \propto (\hat{R} - \hat{R}^{(0)})$ and a, b are real constants with $a^2 \ll 1$ (cf. Deane *et al.* 1987). The system (6.2) possesses a trivial solution $r_1 = r_2 = 0$ which is unstable for $\lambda > 0$, together with four non-trivial steady solutions: $r_1 = 0, r_2^2 = \lambda$ and $r_2 = 0, r_1^2 = \lambda$ (travelling waves), $r_1^2 = r_2^2$ (standing wave) and $r_1^2 + r_2^2 = -a/b$ ($r_1^2 \neq r_2^2$, $a/b < 0$, modulated wave). Figure 10 shows bifurcation diagrams for the system (6.2)

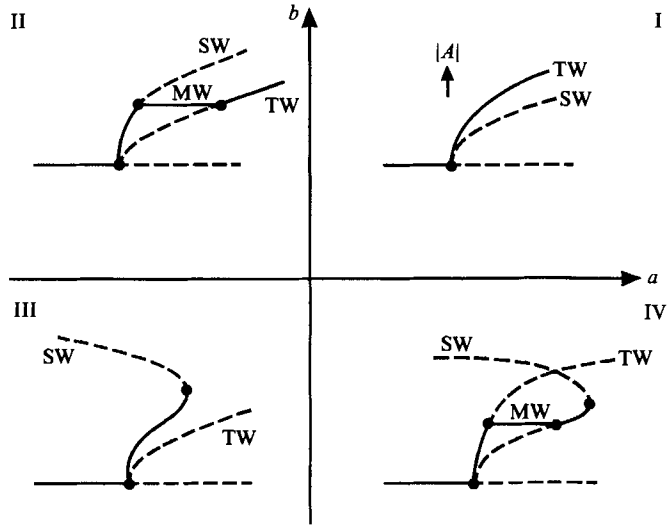

FIGURE 10. Bifurcation diagrams for standing waves and travelling waves in the (a, b)-parameter plane for the system (6.2). Each diagram shows the amplitude $|A|$ plotted against the control parameter λ for standing wave (SW), travelling wave (TW) and modulated wave (MW) solutions. Full lines indicate stable solutions and broken lines indicate unstable solutions.

in different quadrants of the (a, b)-plane with the total amplitude $A = (r_1^2 + r_2^2)^{\frac{1}{2}}$ plotted against λ. In the neighbourhood of the bifurcation at $\lambda = 0$, standing waves are stable if $a < 0$ and travelling waves are stable if $a > 0$; moreover the solution that is stable has the greater value of A^2 (Knobloch *et al.* 1986). Note that $A^2 \propto E_{\max}$ for standing waves while $A^2 \propto 2E$ for travelling waves.

Our results for $\hat{\beta} = 32$ correspond to quadrant II of figure 10. For $(\hat{R} - R^{(0)})$ small (case 32C) standing waves are stable and $E_{\max}/2E \approx 1.06$, where E is the kinetic energy of the travelling wave solution. In case 32D, stability has been transferred to the travelling wave solutions so modulated waves must exist for some Rayleigh numbers in the range $1.11 < \hat{R}/\hat{R}^{(0)} < 2.22$. For $\hat{\beta} = 8$ standing waves are still stable in the neighbourhood of the Hopf bifurcation but for case 8C we found $E_{\max}/2E \approx 0.48$, suggesting that higher-order terms have become significant in the evolution equations. The reference atmosphere defined in §2.2 is stable for all $\hat{R}$ if $\hat{\beta} \leqslant 3$. It is, however, possible to choose m and z_0 so that convection occurs for lower values of $\hat{\beta}$ and there may then be a transition to a regime in which travelling waves are preferred (corresponding to quadrant I of figure 10). If $\hat{\beta}$ is increased from $\hat{\beta}^{(0)}$ for some fixed $\hat{R} > 15000$ we expect travelling waves to be stable in the neighbourhood of the oscillatory bifurcation.

With $\hat{\beta} = 64$ we found a modulated wave solution (case 64D) which apparently did not develop into a steady travelling wave as $\hat{R}$ was increased. We suggest that the results for $\hat{\beta} = 128$ correspond to quadrant III of figure 10, with a 'stable' standing wave solution for all $\hat{R}$ (the turning point might be removed by adding suitable higher-order terms to (2.3)). Behaviour is, however, made more complicated by spatial modulation of the standing waves. This involves narrower rolls, corresponding to $\lambda = \frac{1}{2}$, which are not represented in (6.2). That interaction leads to further bifurcations which we shall ignore here, though they will be mentioned in §7.

We saw from figure 1(*b*) that if $\hat{R}$ is increased from $\hat{R}^{(0)}$ for fixed $\hat{\beta}$ then the oscillatory branch and the steady branch can remain separate over the range with

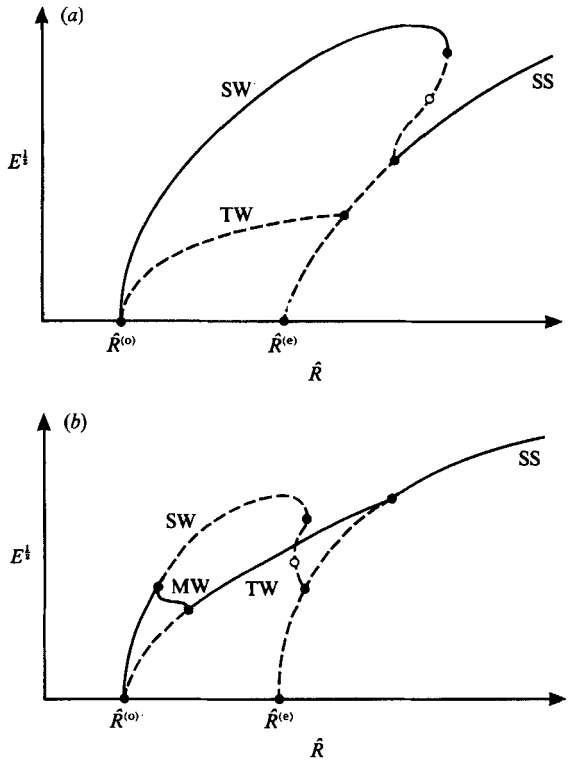

FIGURE 11. The relationship between branches of standing wave, travelling wave and steady solutions as $\hat{R}$ is increased for fixed Q. Schematic bifurcation diagrams showing $E^{\frac{1}{2}}$ as a function of $\hat{R}$ for cases where (*a*) standing waves (SW) are always stable and (*b*) standing waves transfer stability to travelling waves (TW) through a branch of modulated waves (MW). Steady solutions (SS) are stable for large $\hat{R}$. Filled circles and hollow circles denote local and global bifurcations respectively.

which we are concerned. On the other hand, if $\hat{R}$ is increased for fixed Q then $\hat{\beta}$ increases until, from figure 1 (*a*), $\hat{R} = \hat{R}^{(e)}$ for some value of $\hat{\beta}$. Thus it is appropriate to consider also the relationship between the branches of travelling wave, standing wave and steady solutions. By analogy with Boussinesq magnetoconvection with $\lambda = 1$, we expect the steady branch to bifurcate (subcritically) in the direction of increasing $\hat{R}$ (Proctor & Weiss 1982). The standing wave branch terminates in a Hopf bifurcation from the steady branch, while the travelling wave branch terminates in a pitchfork bifurcation. The appropriate bifurcation diagrams are sketched in figures 11 (*a*) and 11 (*b*) which correspond to the cases in quadrants III and II of figure 10 (cf. cases III$^-$ and IX$^-$ of figure 8 in Dangelmayr & Knobloch 1987). Note, however, that these schematic diagrams are grossly simplified. The numerical experiments indicate that there are further bifurcations leading to chaotic oscillations with asymmetric spatial structure.

The properties of the travelling waves are broadly consistent with our assertion that they only occur where the magnetic pressure is significant. Solutions of the type shown in figures 6 and 7 were only found for $F > 0.03$ ($\hat{\beta} < 60$). From table 4 the travelling waves all showed significant evacuation of regions where the field was strong, with reductions of up to 70% in density and local Mach numbers, as defined in (4.2), of up to 0.5. We made two further runs, both for case 32F, to investigate

whether travelling waves were sensitive to changes in diffusivities. The first, with $\sigma = 1$ instead of $\sigma = 0.1$, yielded travelling waves with a similar value of N but lower kinetic energy. The second, with $\zeta = 0.3$ instead of $\zeta = 0.1$ and a corresponding reduction in Q, led to a standing wave solution.

As pointed out in §5, the phase velocity v of the waves is relatively low. The results in table 4 suggest that if $\hat{\beta}$ is fixed v tends to a limit $\tilde{v}$ as $\hat{R}$ is increased. In this limit $\tilde{v}$ increases with increasing F though it remains significantly smaller than either the sound speed v_S or the Alfvén speed v_A. For our reference atmosphere $v_S = (\gamma z)^{\frac{1}{2}}$ so that $0.53 \leqslant v_S \leqslant 1.39$ and $\hat{v}_S \approx 1.05$. In figure 9(*b*) we plot the velocity $\tilde{v}$ of the travelling waves against the Alfvén speed $\hat{v}_A = \hat{\Phi}\hat{v}_S$. The curve is roughly consistent with a linear relationship of the form $\tilde{v} \approx 0.6\hat{v}_A$, though its slope decreases with increasing $\hat{v}_A$.

In the Boussinesq limit the velocity of undamped travelling waves is given by (5.2). It can be shown that the velocity of travelling waves in Boussinesq magnetoconvection, at the oscillatory bifurcation where they are marginally stable, is given by the same expression, $v = \frac{1}{2}\lambda v_A$, provided $\sigma, \zeta \ll 1$. For $\lambda = 1$ travelling waves therefore have a velocity $v = \frac{1}{2}v_A$. Note that the product $v\tau = \lambda$, from (5.2) and (6.1): the time taken by a travelling wave to cross the domain is equal to the period of a standing wave, which is just the time taken for a disturbance to traverse twice the layer depth (a full wavelength) in the vertical direction.

The fact that travelling waves in compressible magnetoconvection have approximately the same velocity as that given by (5.2) for $32 \geqslant \beta \geqslant 6$ provides further support for our assumption that they are essentially slow magnetoacoustic waves. On the other hand, their detailed structure is dominated by regions of strong field, where magnetic pressure is significant. From table 4, the peak value of the magnetic pressure $P_{m,\max} \geqslant 0.3$ in all cases where travelling waves are stable. In the nonlinear regime compressible effects not only lead to a preference for travelling waves but also determine their spatial structure.

7. Mixed-mode solutions ($\lambda = 2$)

In this section we discuss the behaviour of solutions with $\lambda = 2$ in that region of the $(\hat{\beta}, \hat{R})$-plane where standing wave and travelling wave solutions are expected to exist. For a given value of $\hat{R}$ the Hopf bifurcation occurs at $\hat{\beta} = \hat{\beta}^{(o)}$ and steady solutions exist only for $\hat{\beta} > \hat{\beta}_{\min}$. We shall study the different types of time-dependent behaviour found as $\hat{R}$ is increased for a fixed value of $\hat{\beta}$ such that $\hat{\beta}_{\min} > \hat{\beta} \geqslant \hat{\beta}^{(o)}$. As we saw in §4, symmetrical standing waves with two rolls are stable immediately above the Hopf bifurcation at $\hat{R} = \hat{R}^{(o)}$. For $\hat{\beta}$ sufficiently small and $\hat{R}$ sufficiently large there is, however, a transition to travelling waves with four rolls in the domain. This involves both a change of scale and a change in the form of the solution. In what follows we shall try to identify the bifurcations that are involved.

We focus our attention on runs with $\hat{\beta} = 8$. When $\hat{R} \approx 2\hat{R}^{(o)}$ the fundamental standing wave solution is still stable. The solution for case 8B, illustrated in figures 4 and 5(*b*), is strictly periodic in time with period τ and possesses two important symmetries. At any instant the solution is mirror-symmetric about a plane $x = x_0$ (where x_0 depends on the initial conditions only) and, since it is periodic in x, about the plane $x = x_0 + \frac{1}{2}\lambda$. There is also a translational symmetry

$$(x, t) \to (x + \tfrac{1}{2}\lambda, t + \tfrac{1}{2}\tau), \tag{7.1}$$

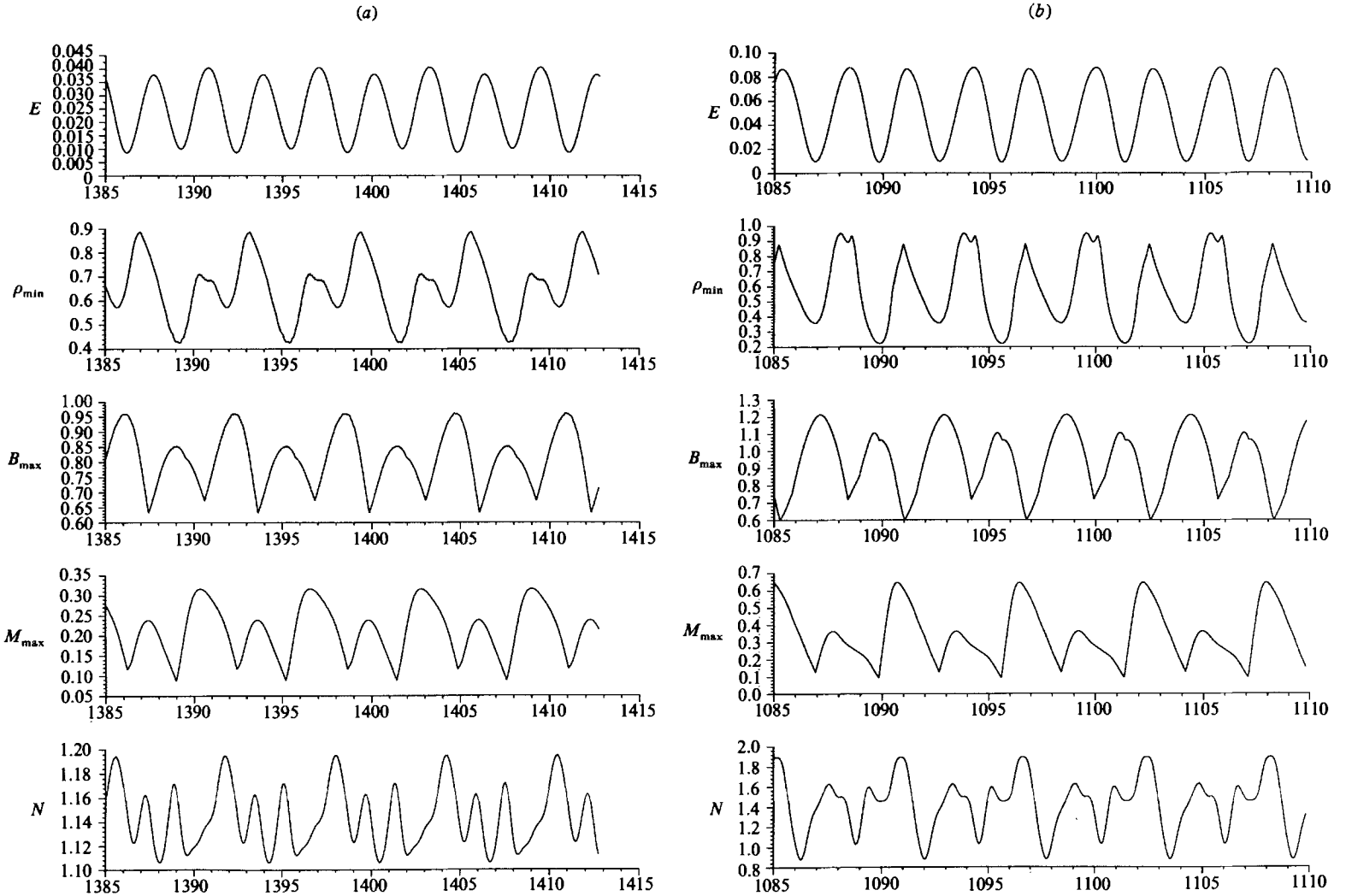

FIGURE 12. Time traces for modulated wave solutions ($\lambda = 2$). As figure 5 but for (*a*) case 8C and (*b*) case 8D.

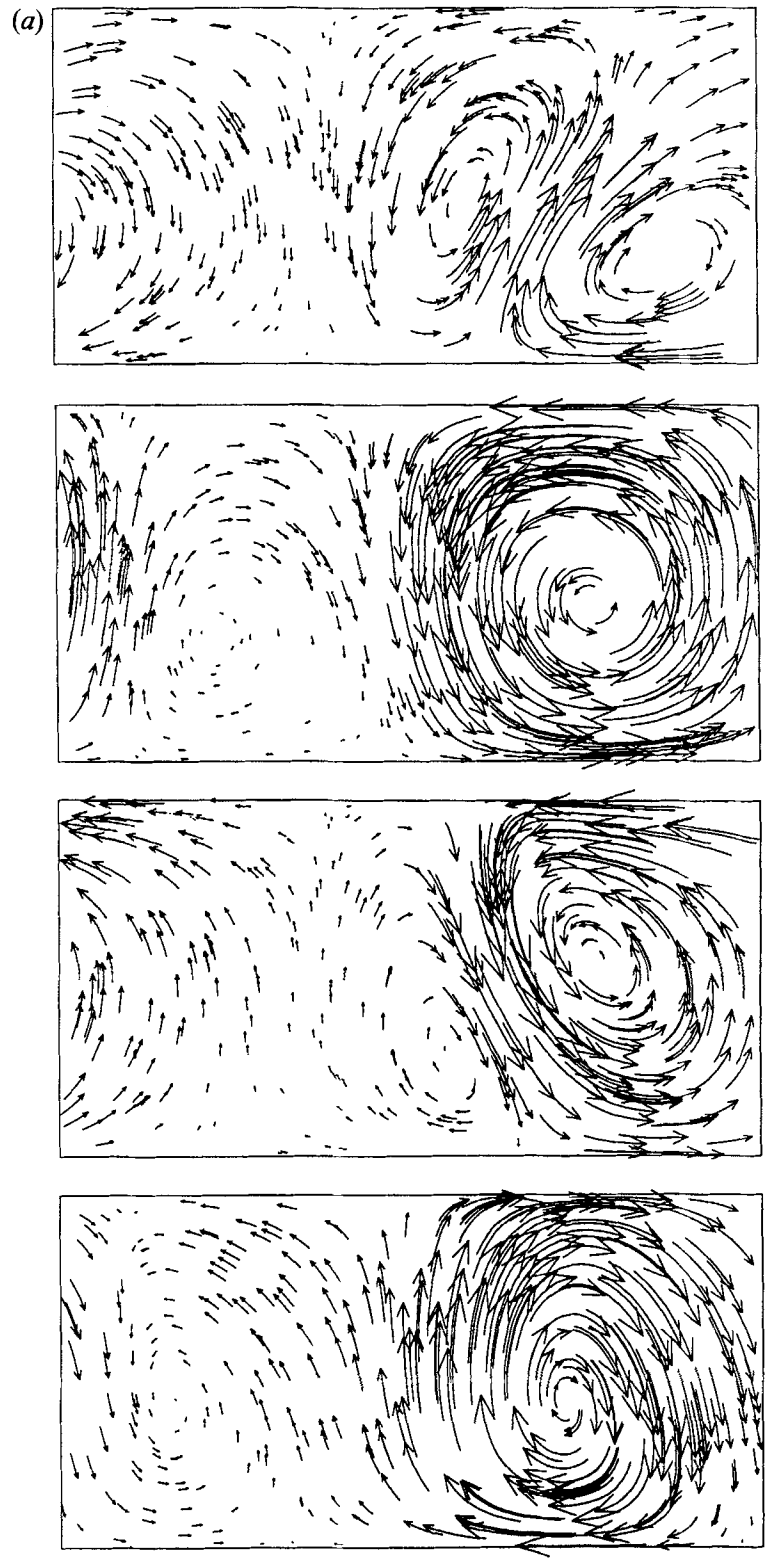

FIGURE 13(a). For caption see facing page.

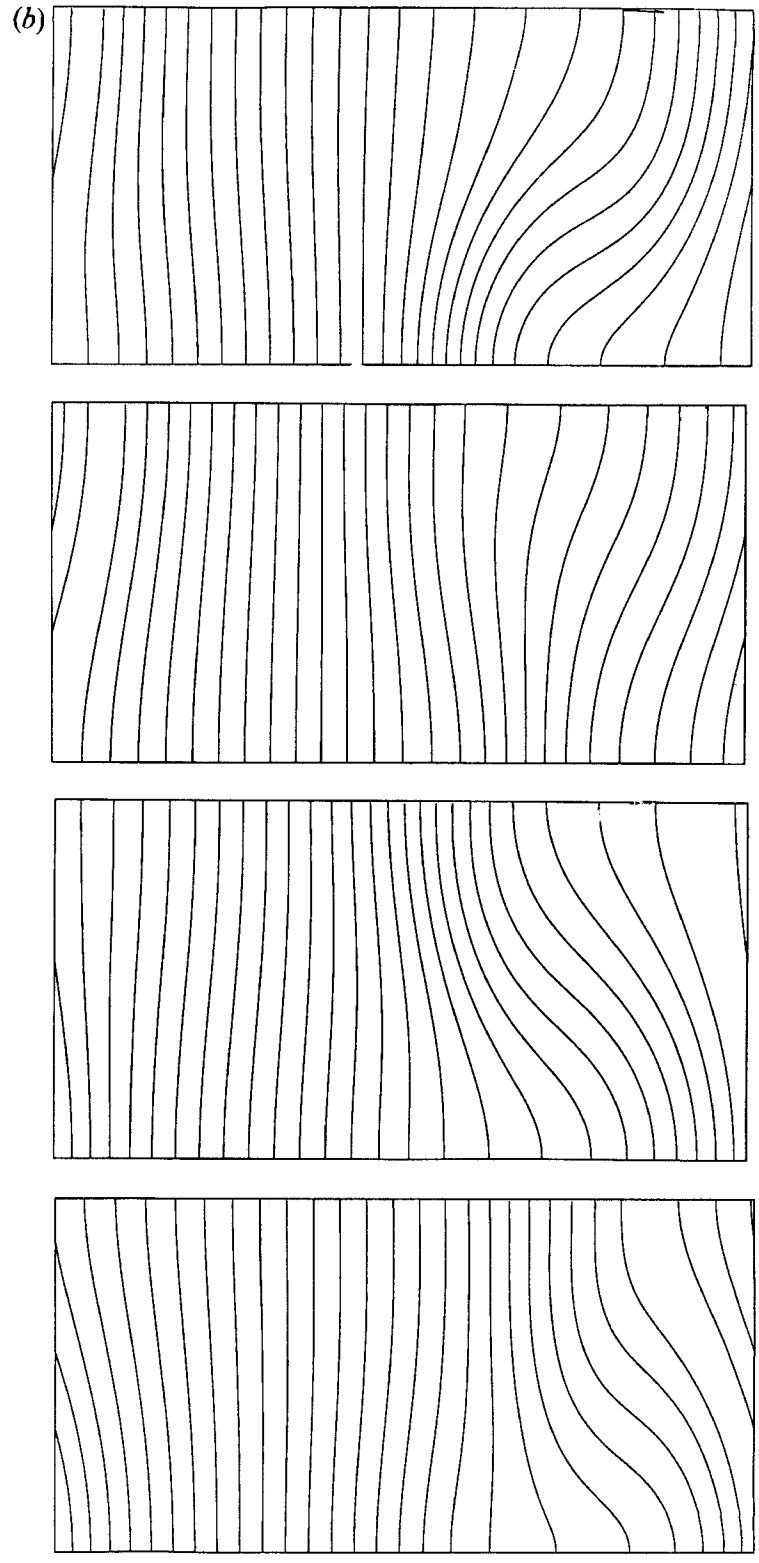

FIGURE 13. Mixed-mode travelling wave solutions for case 8C. (*a*) Velocity streaklines and (*b*) magnetic field lines at equally spaced intervals. The waves propagate towards the right, with maximum amplitude around $x = 0.77\lambda$.

corresponding to displacement by half a period in space and time. (Symmetry between upward and downward plumes is absent in a stratified layer.)

There is also a branch of travelling wave solutions that emerges from the bifurcation at $\hat{R}^{(o)}$ but solutions on this branch apparently remain unstable for $\hat{R}^{(o)} < \hat{R} \lesssim 2\hat{R}^{(o)}$. The waves travel to the right or left without change of form at a speed v and therefore violate the mirror symmetry of the standing wave solutions. The travelling wave solutions repeat themselves exactly after an interval $\tau = \lambda/v$ and possess the symmetry $(x, t) \rightarrow (x \pm vt_0, t + t_0)$ for any t_0; in particular they preserve the translational symmetry (7.1) for $t_0 = \frac{1}{2}\tau$.

In addition to these pure solutions with two rolls in the box there are pure four-roll solutions for $\hat{R}$ sufficiently large: these are just the standing wave and travelling wave solutions discussed in §6. The pure two-roll solutions lose symmetry at bifurcations giving rise to branches of mixed-mode solutions linking the branches of pure two-roll and four-roll solutions. Mixed-mode oscillations appear in Boussinesq magnetoconvection with mirror symmetry imposed at $x_0 = 0$ (Weiss 1981*b*) and the relationship between the different branches has been investigated in some detail (Nagata, Proctor & Weiss 1989). The translational symmetry (7.1) is broken when mixed-mode solutions bifurcate from pure two-roll solutions in the Boussinesq approximation. In our problem mirror symmetry may also be broken and travelling waves can appear.

A run for case 8C was started by slightly perturbing the static solution and it initially developed into symmetrical oscillations with a period $\tau \approx 5.6$ and peak values of E and N significantly higher than those for case 8B. This standing wave solution proved unstable and there was a gradual transition (by time $t \approx 800$) to an almost periodic solution for which both mirror symmetry and translational symmetry are broken. Time traces for this solution are displayed in figure 12(*a*). Comparing them with those for case 8B in figure 5(*b*) we note that the peak values of E, N, $B_{\max}$ and $M_{\max}$ are all lower for case 8C although the Rayleigh number has been doubled. The new solution varies with a period $\tau \approx 6.2$ and successive half-cycles are quite different. The kinetic energy varies in the range $33 \geqslant E \geqslant 7$, without dropping to zero, suggesting the presence of a modulated travelling wave. Streaklines and magnetic field lines are illustrated in figure 13. Motion is dominated by a single roll which reverses its sense of motion and the solution apparently repeats almost exactly after an interval τ has elapsed. This dominant eddy is centred at $x \approx 0.77\lambda$ and it distorts the magnetic field in the region $0.5 \leqslant x/\lambda \leqslant 1.1$; a second, weaker roll appears in a region of stronger field and for $0.1 \leqslant x/\lambda \leqslant 0.5$ the field lines are only slightly distorted by the motion. In the course of the oscillation the rolls move slowly to the right in figure 13, travelling approximately one wavelength during the period τ. Moreover, they have a slightly triangular structure with prograde velocity at the vertices, which point alternately upwards and downwards. Apparently we have a two-roll travelling wave solution, modulated in both space and time. To a first approximation, the modulation remains fixed in space and the kinetic energy varies as the rolls drift by, with unequal maxima since clockwise and anticlockwise rolls are not equivalent.

Closer inspection of these solutions reveals that they are not periodic. For example, a trajectory plotted in the phase plane with coordinates $w(0, \frac{1}{2}, t)$ and $B_z(0, \frac{1}{2}, t)$ is not attracted to a limit cycle but instead describes a torus. Over a long interval the position of the dominant eddy drifts gradually to the left across the box, with a velocity $\delta v \approx 6.2 \times 10^{-4}$, so that the spatial modulation pattern moves a distance λ in a time $\lambda/\delta v \approx 520\tau$. Apparently this solution is quasi-periodic, with one frequency

associated with the rate at which travelling waves cross the box and a very much smaller frequency of modulation.

This pattern can be ascribed to interference between travelling waves with wavelengths λ and $\frac{1}{2}\lambda$. In the Boussinesq limit these waves travel with velocities v and $\frac{1}{2}v$ respectively in the linear regime. Hence we might consider a combination of the form

$$u(x,z,t) = [\sin a(x-vt) + \epsilon \sin 2a\{x-\tfrac{1}{2}(v-\delta v)\,t\}]\cos \pi z, \tag{7.2}$$

where $a = 2\pi/\lambda$, $v = \frac{1}{2}\lambda v_A$ and $\delta v \ll v$. This can be written as

$$u = [\{1+2\epsilon \cos a(x+\delta v t)\}\sin a(x-vt) + \epsilon \sin a(v+\delta v)\,t]\cos \pi z. \tag{7.3}$$

Thus two waves travelling in the same direction give rise to a modulated solution with period $\tau \approx \lambda/v$. The solution would be periodic if the four-roll wave travelled at exactly half the speed of the two-roll wave and the entire pattern would then repeat after an interval $\tau = 2/v_A$. For a compressible layer with $\hat{\beta} = 8$ the Alfvén speed $\hat{v}_A \approx 0.41$ and the corresponding period $\tau \approx 4.9$, from (6.1). Pure four-roll travelling waves have a velocity $v \approx 0.2\lambda$, while standing waves have a period $\tau \approx 5.5$ (cf. tables 2–4). Apparently the ratio of the two wave velocities remains close to 0.5 in the nonlinear regime even when the layer is stratified.

A further increase in $\hat{R}$ leads to a different type of solution. Case 8D provides an example of a strictly periodic solution which retains mirror symmetry though the translational symmetry (7.1) has been lost. Figure 14 (*a*, *b*) shows streaklines at two stages when the kinetic energy is a maximum, separated by half a period. The two rolls are separated by symmetry planes at $x = x_0, x_0+\frac{1}{2}\lambda$, where $x_0 \approx 0.39\lambda$. In the neighbourhood of $x = x_0$ the magnetic field is strongly distorted by the motion but convection is inhibited around $x = x_0+\frac{1}{2}\lambda$, where the field is relatively undistorted, as shown by the field lines when $B_{\max}$ is a maximum, plotted in figure 14 (*c*, *d*). The oscillation has a period $\tau \approx 5.8$ and alternate half-cycles are quite different (since upward and downward motion at $x = x_0$ are not equivalent). In the time traces in figure 12 (*b*) alternate peaks in N, $M_{\max}$, $B_{\max}$ and $\rho_{\min}$ have quite different shapes, though the kinetic energy E shows only slight asymmetry. The amplitude of the oscillations is somewhat greater than for case 8B and much greater than for case 8C in figure 12 (*a*). This solution is a compressible analogue of the asymmetric oscillations found in Boussinesq magnetoconvection with $R = 10^4$ and $\sigma = 1$. In those results a strong flux sheet was formed between each pair of rolls and the motion and field became increasingly segregated as Q decreased (cf. figure 6 of Weiss 1981*b*). Here further increases of $\hat{R}$ lead to pure four-roll travelling wave solutions for cases 8E and 8F as we saw in §§5 and 6.

The mirror-symmetric oscillation for case 8D presumably lies on a branch of periodic mixed-mode solutions that bifurcates from the branch of pure two-roll standing wave solutions. In the Boussinesq limit the period $\tau = 2/v_A$ of linear standing waves is independent of the aspect ratio λ and figure 9 (*a*) shows that this remains a good approximation for slow magnetoacoustic oscillations with $\hat{\beta} = 8$. Thus the asymmetric periodic oscillations in figure 14 can be regarded as a combination of pure two-roll and pure four-roll standing wave solutions which have the same period and are locked in phase.

When $\hat{\beta} = 6$ the transition from a two-roll standing wave to a four-roll travelling wave is more straightforward. Case 6B yields a stable symmetric oscillatory solution which gives way to mixed-mode travelling waves as $\hat{R}$ is increased. In case 6C small perturbations developed into a symmetrical standing wave ($\tau \approx 5.0$) which became

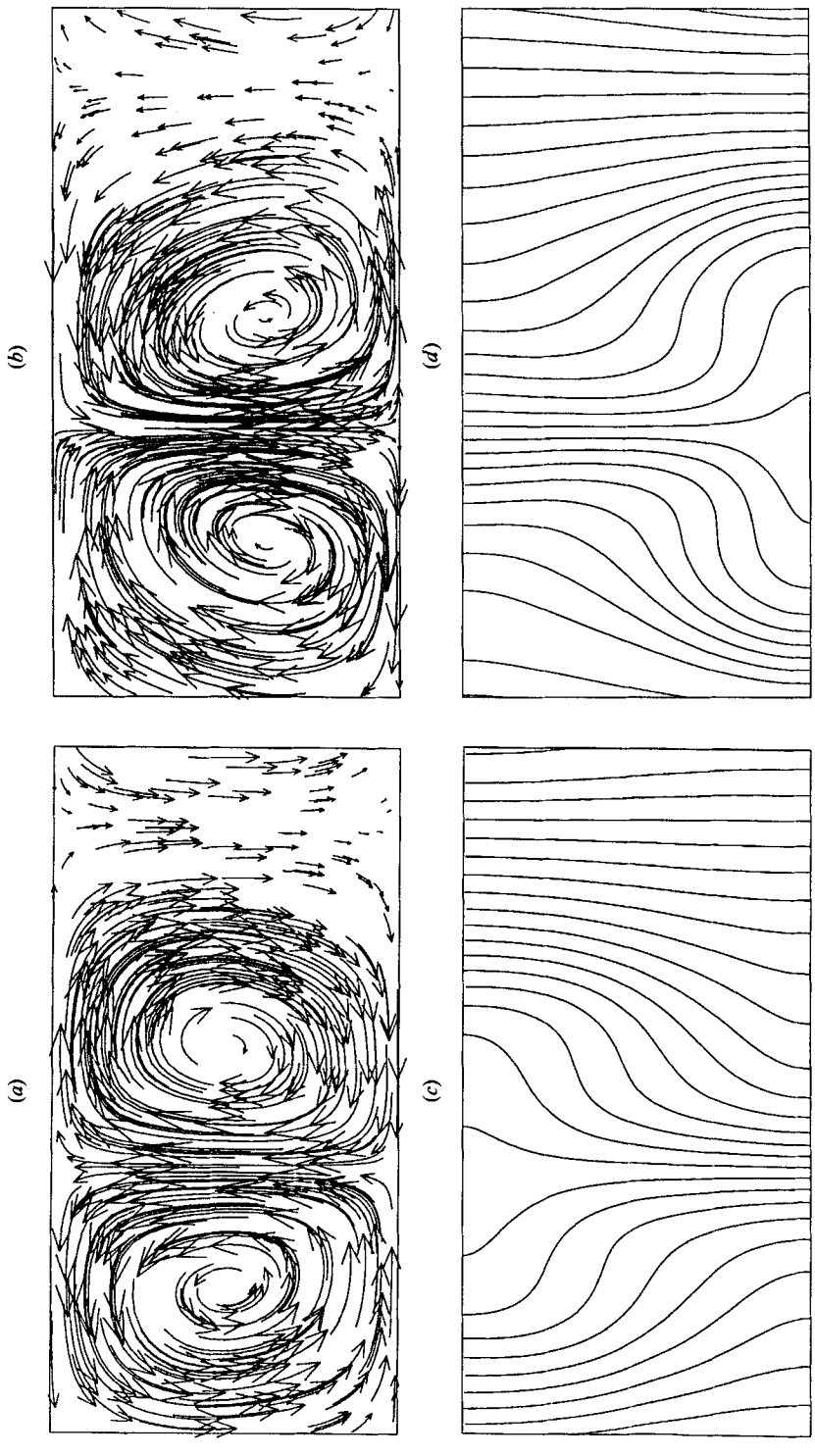

FIGURE 14 Mixed-mode periodic behaviour for case 8D. (*a*, *b*) Velocity streaklines when E is near a maximum and (*c*, *d*) magnetic field lines when $B_{\max}$ is near a maximum. This solution retains mirror symmetry about the planes $x/\lambda = 0.39, 0.89$. (*a*, *b*) and (*c*, *d*) are separated by half a period.

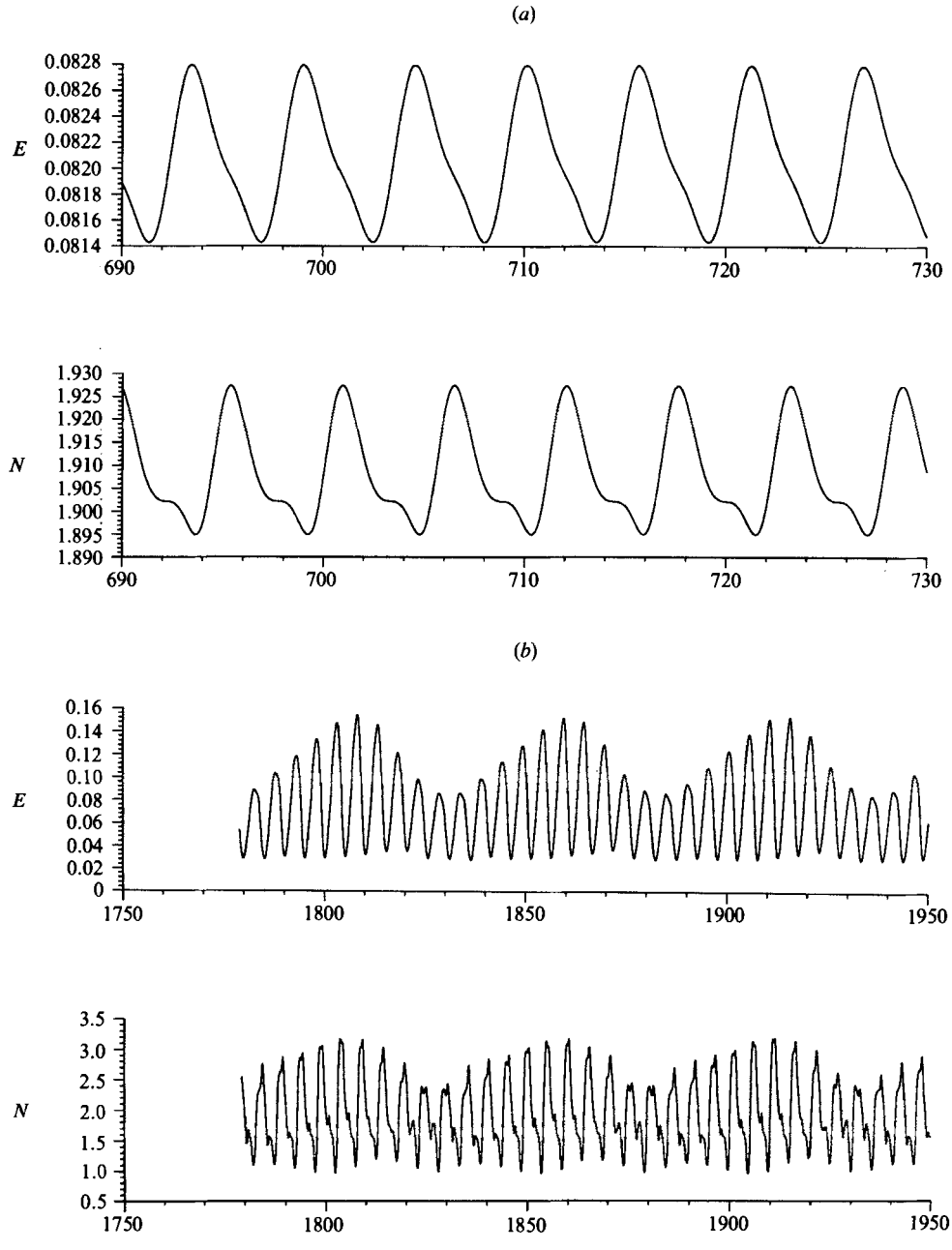

FIGURE 15. Modulated waves ($\lambda = 2$). (*a*) Variation with time of E and N for the modulated travelling wave solution in case 6D. (*b*) As (*a*), showing quasi-periodic behaviour for case 32E.

unstable and was superseded by an almost periodic solution ($\tau \approx 5.3$) lacking both mirror and translational symmetries. As in case 8C motion is dominated by a single eddy that reverses and closer inspection reveals an asymmetrically modulated two-roll pattern that drifts with an average velocity $v \approx \lambda/\tau$. The rolls have a clear triangular structure with prograde velocity at the upward- and downward-pointing vertices and the pattern again corresponds to a mixed-mode solution involving two-

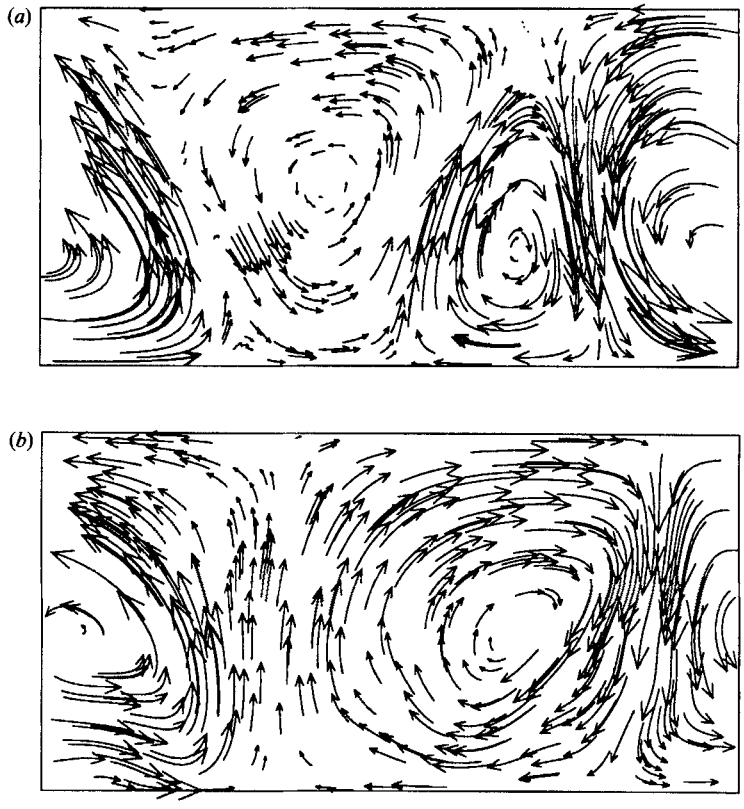

FIGURE 16. Quasi-periodic spatially modulated behaviour. Streaklines for case 32D showing different phases with (*a*) three rolls and (*b*) two rolls present in the box.

roll and four-roll travelling waves. The spatial modulation pattern drifts very slowly, with a velocity $\delta v \approx 2 \times 10^{-4}$ indicating that the velocity of travelling waves with $\lambda = 1$ is almost exactly half that of waves with $\lambda = 2$.

As $\hat{R}$ is increased a smaller horizontal scale is preferred. The solution for case 6D is a four-roll travelling wave, slightly modulated in space and time. Figure 15(*a*) shows time traces of the kinetic energy and the Nusselt number. They oscillate periodically with a period $\tau_m \approx 5.6$ and $1.904 \leqslant N \leqslant 1.935$ while E varies by about 1.6%. In an interval τ_m the waves travel a distance $v\tau_m \approx 0.59\lambda$, so the spatial pattern does not repeat after each period of the modulation. In this solution the rolls have a triangular shape similar to that in figure 6 but their amplitude is modulated with a wavelength λ and the modulation pattern is not fixed in space. Finally, a further doubling of $\hat{R}$ leads to pure four-roll travelling waves for case 6E.

No steady travelling wave solutions were found for $\hat{\beta} = 32$, even for runs started from travelling waves with $\hat{\beta} = 8$. On the other hand there was a variety of quasi-periodic and aperiodic behaviour. Case 32C again yielded transient symmetric standing waves which lost stability and gradually developed into apparently quasi-periodic asymmetric oscillations. In this solution there are two counter-rotating rolls, one of which is usually more prominent than the other. Although there is no plane of symmetry between the rolls they reverse cyclically without drifting horizontally across the box. The mean cycle period $\bar{\tau}$ and the modulation period τ_m appear incommensurate, with $\tau_m \approx 2.4\bar{\tau}$. The asymmetric spatial modulation suggests that

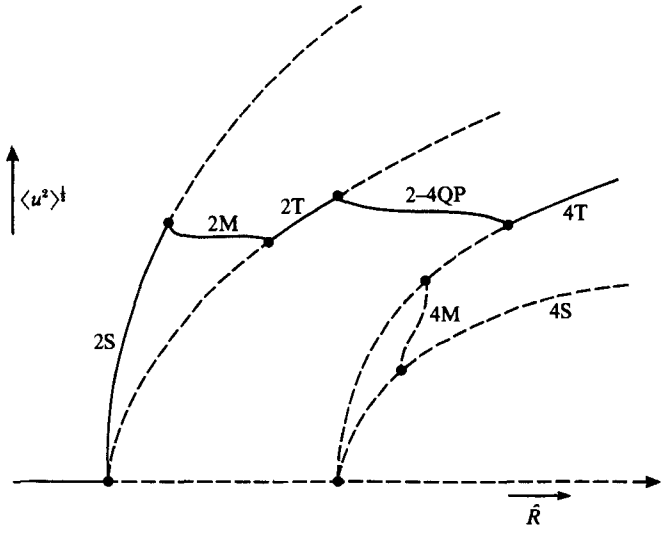

FIGURE 17. Schematic bifurcation diagram for $\hat{\beta} = 6$. Solution branches are sketched in the $(U, \hat{R})$-plane, where U is the r.m.s. velocity. Full lines indicate stable solutions and broken lines unstable solutions. The different branches of pure two- and four-roll standing (S), travelling (T) and modulated (M) waves are labelled, together with mixed-mode quasi-periodic (2–4 QP) solution branches. All bifurcations are assumed to be supercritical.

this is a mixed-mode quasi-periodic solution involving two-roll and four-roll standing waves.

Increasing $\hat{R}$ led to more complicated quasi-periodic solutions. In case 32D there are sometimes two asymmetric rolls, more often three and occasionally four. Figure 16 shows two extreme cases: in figure 16(*a*) there are three rolls with a triangular structure reminiscent of travelling waves but in figure 16(*b*) the two rolls are more nearly square as in standing wave solutions. Apparently the four-roll component is drifting relative to the oscillatory two-roll component, suggesting that this mixed-mode solution involves a two-roll standing wave and a four-roll travelling wave which are not locked in phase.

Case 32E displays more striking quasi-periodic modulation, as indicated by the time traces of E and N in figure 15(*b*). The velocity pattern reveals two prominent rolls, reversing without mirror symmetry and showing considerable structure when the kinetic energy is low. Its structure again suggests that there is a two-roll standing wave modulated by a four-roll travelling wave component.

Finally, case 32F yielded aperiodically modulated behaviour with signs of intermittency. By this value of $\hat{R}$ the static solution is unstable to rolls with $\lambda = 2$, $1, \frac{2}{3}$ and is about to become unstable for $\lambda = \frac{1}{2}$, so more complicated mixed-mode oscillations may arise. Solutions for cases 128C and 128E are also aperiodic, though they are probably related to a branch of mixed-mode solutions that bifurcates from the unstable steady branch.

This survey has revealed a variety of time-dependent mixed-mode solutions, involving standing waves and travelling waves with wavelengths λ and $\frac{1}{2}\lambda$. For $\hat{\beta} \leqslant 8$ there is a transition from a pure two-roll standing wave solution to a pure four-roll travelling wave solution but for $\hat{\beta} \geqslant 32$ the transition is from a standing wave to aperiodic mixed-mode oscillations. Indeed, aperiodic solutions appear even in the Boussinesq approximation at large R (Weiss 1981*c*).

The results for $\hat{\beta} = 6$ are consistent with the schematic bifurcation structure depicted in figure 17. Two-roll standing wave and travelling wave solutions bifurcate from the static solution at $\hat{R} \approx 3500$; initially the standing wave solution is stable but stability is transferred to travelling waves by a branch of two-roll modulated waves. The travelling wave solution becomes unstable to four-roll perturbations and a branch of mixed-mode travelling wave solutions emerges from a Hopf bifurcation. These solutions are quasi-periodic and develop into modulated four-roll travelling waves, on a branch that bifurcates from that of pure travelling wave solutions around $\hat{R} \approx 40000$. For simplicity this picture assumes a minimal number of bifurcations, all of which are supposed to be supercritical. The behaviour found for $\hat{\beta} = 8, 32$ involves more solution branches and the bifurcation structure is correspondingly more intricate.

One curious feature of the results for $\hat{\beta} = 6$ and $\hat{\beta} = 8$ is the appearance of solutions that seem at first sight to be periodic but are actually quasi-periodic. In the Boussinesq approximation slow magnetoacoustic waves have a velocity $\frac{1}{2}\lambda v_A$ relative to the preferred inertial frame in which the total momentum vanishes, so their frequency $\omega = \pi v_A$ is independent of λ. One might naively expect phase-locking in the nonlinear regime but since the system is invariant with respect to displacements in the x-direction the phase of the two-roll wave is an ignorable order parameter. Hence there is no frequency entrainment (cf. Rand 1982). On the other hand, both two-roll and four-roll waves have very similar frequencies, which change only slightly in the nonlinear regime, so the velocity difference δv in (7.2) remains small. Moreover, δv is less when $\hat{\beta} = 6$, close to the stability boundary in figure 1(*b*), than it is for $\hat{\beta} = 8$.

8. Conclusion

In this paper we have tried to explore the connections between two-dimensional standing wave and travelling wave solutions in spatially periodic boxes with aspect ratios $\lambda = 1, 2$. When convection first sets in standing wave solutions are preferred and two-roll solutions with $\lambda = 2$ are stable to four-roll perturbations. For $\hat{\beta} > 32$ we found no travelling wave solutions though time-dependent solutions showed complicated spatial and temporal modulation at high Rayleigh numbers. Stable travelling wave solutions with $\lambda = 1$ exist for $32 \geqslant \hat{\beta} \geqslant 6$ and $\hat{R} \geqslant 16000$. When $\lambda = 2$ the two-roll standing wave solutions become unstable for $\hat{R} \geqslant 8000$ and stability is transferred to four-roll travelling wave solutions when $\hat{\beta} \leqslant 8$. This process involves mixed-mode travelling wave solutions and requires a complicated sequence of bifurcations.

Our most significant result is that travelling waves are preferred when $\hat{\beta}$ is sufficiently small and $\hat{R}$ sufficiently large. This is an essentially compressible effect, though the waves travel as slow magnetoacoustic trapped modes even in the nonlinear regime. We have discussed some mathematical aspects of the associated bifurcation structure but it is also important to establish the physical mechanisms that lead to the appearance of stable travelling waves.

Travelling waves exist because the boundary conditions at $z = 0, 1$ provide a waveguide. In the Boussinesq regime slow magnetoacoustic waves are reflected at the upper and lower boundaries and interfere to give waves travelling to left or right with a velocity $v = \frac{1}{2}\lambda v_A$. These waves can in turn combine to yield standing waves with a period $\tau = 2/v_A$. Our results show that the velocity and period of travelling

wave and standing wave solutions are those of slow magnetoacoustic modes even when $\hat{\beta}$ is relatively small.

Linear theory explains the existence of travelling waves but we must turn to nonlinear theory in order to discover whether standing waves or travelling waves are preferred. In some cases (e.g. where relative rates of diffusion are crucial) this question can only be answered by a detailed calculation. In others we may hope to find a criterion based on physical arguments. We might begin by seeking a propulsion mechanism. Energy propagates with the group velocity V and for slow magnetoacoustic waves in the Boussinesq limit V is parallel to the magnetic field. Thus we should expect that travelling waves will be preferred in the presence of an imposed horizontal magnetic field, where $V = v_A \hat{\boldsymbol{x}}$ (cf. Parker 1984), while standing waves will be preferred with a vertical field ($V = v_A \hat{\boldsymbol{z}}$). Detailed calculations have confirmed that travelling waves are stable in a horizontal field (Knobloch 1986) and that standing waves are preferred in a vertical field with λ of order unity (Dangelmayr & Knobloch 1986). On the other hand, Proctor (1986) found that for $Q \gg 1$, when convection first appears with $\lambda = O(Q^{-\frac{1}{6}})$, travelling waves are initially stable; in that regime diffusion is important. In other systems the situation is less clear. Travelling waves are preferred in thermosolutal or binary convection, while standing waves have been found in experiments with a rotating system, but there is no obvious criterion based on group velocities since V is perpendicular to the wave vector for internal gravity waves and for inertial waves.

Our discussion of group velocity has so far relied on the Boussinesq approximation, which is valid only for weak magnetic fields with $\hat{\beta} \gg 1$. In that limit we find standing waves, supported entirely by magnetic tension. As $\hat{\beta}$ is decreased compressional effects become significant and the group velocity acquires a component perpendicular to the imposed magnetic field. Thus there exists a possible propulsion mechanism for travelling waves when $\hat{\beta}$ is of order unity. If the field strength is further increased so that $\hat{\beta} \ll 1$ slow magnetoacoustic waves have a group velocity $V = v_S \hat{\boldsymbol{z}}$ and we again expect that standing waves will be preferred. Apparently stable travelling waves are likely to be found only in the regime where the sound speed and the Alfvén speed are comparable.

Fast magnetoacoustic waves travel almost isotropically at a speed $v \geqslant v_S$ and the sound speed $\hat{v}_S > 2.25\hat{v}_A$ in our numerical experiments, where travelling waves propagate as slow magnetoacoustic waves with $v < 0.22\hat{v}_S$. Nevertheless, pressure fluctuations are important in compressible magnetoconvection. In the nonlinear regime convective motion leads to local concentrations of magnetic flux where the magnetic pressure P_m becomes comparable with the ambient gas pressure. In cases where travelling waves were stable P_m reached a peak value in the range $0.30 \leqslant P_{m,\max} \leqslant 0.92$. The gas pressure rises from 0.17 at the top to 0.94 at the middle of the layer, so large local increases in magnetic pressure cannot be balanced by partial evacuation of the flux sheets and consequent reductions in thermal pressure. As a result there is an excess of total pressure Π in regions where the field is strong. Figure 4(*e*) shows that the pressure fluctuations Π' attain local maxima along the jet, which coincides with flux concentrations in figure 6. These fluctuations in total pressure accelerate the fluid in such a way as to produce travelling waves. We believe therefore that pressure fluctuations are responsible both for the transfer of stability from standing to travelling waves and for the triangular form of the travelling wave solutions. When $\hat{\beta}$ is large increases in P_m can be balanced by reductions in P so that Π' remains relatively small. For strong fields (with $\hat{\beta} \leqslant 32$ and $F > 0.05$) convective

motion leads to pressure fluctuations that can only be balanced by inertial terms in the equation of motion. The resulting dynamical interaction leads to low-amplitude travelling waves, propagating as slow magnetoacoustic waves at a rate determined by the Alfvén speed based on the mean field strength.

Standing waves still exist in the nonlinear compressible regime, just as travelling waves exist in Boussinesq magnetoconvection. In oscillatory solutions with mirror planes at $x = x_0, x_0 + \frac{1}{2}\lambda$ the balance between pressure fluctuations and inertial terms must be very delicate. If the mirror symmetry is broken in such a way that alternate rolls are separated by surfaces inclined at angles $\pm\theta$ to the vertical the fluctuations $\Pi'(x, z, t)$ presumably act to drive a jet along the surfaces so that θ increases to produce a triangular structure, propagating with a speed $v \approx \frac{1}{2}\lambda v_A$. This picture suggests that pressure fluctuations in the low-β regime are responsible both for the instability of standing waves and for the spatial form of travelling wave solutions. Paradoxically, their velocity remains the same as in the Boussinesq regime.

Finally we note that this process provides a mechanism for thermal excitation of travelling waves in vertical as well as horizontal magnetic fields. This would apply to shallow convection zones in stars with strong magnetic fields, where F is large and ζ is small. Sunspot umbrae are more complicated, since the effective value of ζ increases with depth owing to ionization, but this mechanism could excite travelling waves in sunspot penumbrae. The astrophysical implications of our results will be discussed elsewhere.

This research was supported by grants from the Science and Engineering Research Council. We thank Fausto Cattaneo, John Edwards, Douglas Gough, Dan Moore, Henk Spruit and Juri Toomre for advice and comments, and we are grateful to JILA and the Max Planck Institut für Astrophysik for providing facilities and hospitality in Boulder and Munich.

Appendix. The semi-implicit scheme

In our simulations of magnetoconvection with small Prandtl numbers, the time step of our explicit numerical scheme is controlled by the thermal diffusion time. However, the dynamical timescale is much longer, being comparable with the viscous diffusion time. Hence it is useful to treat some of the terms explicitly and others implicitly. To illustrate the semi-implicit scheme consider this simple advection–diffusion equation in one dimension,

$$u_t = u_x + \kappa u_{xx}. \tag{A 1}$$

Our explicit Lax–Wendroff scheme would solve this equation in two steps. The first time step advances the solution using forward differences. If δt is the time step and u^n is the value of u at time step n, then this first step has the form

$$u^{n+1} = u^n + \delta t(u_x^n + \kappa u_{xx}^n), \tag{A 2}$$

where the spatial derivatives are represented by centred spatial differences. This provisional step has only $O(\delta t)$ accuracy in time. The second step uses these first-order-accurate values to advance the solution with centred differences

$$u^{n+2} = u^n + 2\delta t(u_x^{n+1} + \kappa u_{xx}^{n+1}) \tag{A 3}$$

thus giving $O(\delta t^2)$ accuracy. For stability the time step of this explicit scheme is limited by both the advective ($\delta t_a \propto 1/\delta x$) and diffusive ($\delta t_\kappa \propto \delta x^2/\kappa$) mesh timescales, where δx is the resolution of the spatial mesh.

In our semi-implicit scheme, the first step remains unaltered. However, the diffusive term is evaluated in the second step using the Crank–Nicolson method. Hence the second step has the form

$$u^{n+2} = u^n + 2\delta t u_x^{n+1} + \kappa \delta t (u_{xx}^n + u_{xx}^{n+2}). \tag{A 4}$$

This semi-implicit method assures stability for time steps larger than δt_κ while retaining the same second-order accuracy as the Lax–Wendroff scheme. For very large time steps the Crank–Nicolson scheme can produce unphysical oscillations which possess very little damping. These oscillations must be negligible over any natural timescale for the solutions to maintain accuracy. For $\delta t \gg \delta t_\kappa$, the amplification factor for one step is $A \approx 1 - \delta t_\kappa / \delta t$. If the smallest natural timescale is $T = N\delta t$ then we must have $A^N \ll 1$. In practice we require $\delta t < (0.2 T \delta t_\kappa)^{\frac{1}{2}}$.

Applying this scheme to equation (2.4) leaves us with a Helmholtz equation with variable coefficients for the temperature, which we solve at each even time step using the method of multiple grids (Brandt 1984). The simplest implementation of this method, where Gauss–Seidel relaxation is used at each level and linear interpolation is used between levels, proved adequate. Our multigrid solver gives solutions accurate to $O(\delta x^2)$ in four V-cycles, each four levels deep, for typical resolution. To assure convergence we used ten cycles in our code.

The resulting semi-implicit code increased the usable time step by more than a factor of three while requiring only 6% more CPU time per step. For the range of parameters we consider, the Courant condition on wave propagation and advection satisfies our accuracy criterion above. The code was tested both against the fully explicit version and against growth rates predicted by linear analysis. In both cases it agreed to within acceptable accuracy.

REFERENCES

Antia, H. M. & Chitre, S. M. 1979 Waves in the sunspot umbra. *Solar Phys.* **63**, 67–78.

Brandt, A. 1984 *Multigrid Methods: 1984 Guide with Applications to Fluid Dynamics.* GMD-Studieren Nr 85, Bonn.

Bretherton, C. S. & Spiegel, E. A. 1983 Intermittency through modulational instability. *Phys. Lett.* **96A**, 152–196.

Cattaneo, F. 1984 Oscillatory convection in sunspots. In *The Hydromagnetics of the Sun* (ed. T. D. Guyenne), pp. 47–50. ESA SP-220.

Chandrasekhar, S. 1961 *Hydrodynamic and Hydromagnetic Stability.* Oxford.

Cowling, T. G. 1976 *Magnetohydrodynamics* (2nd edn). Adam Hilger.

Dangelmayr, G. & Knobloch, E. 1986 Interaction between standing and travelling waves and steady states in magnetoconvection. *Phys. Lett.* **117A**, 394–398.

Dangelmayr, G. & Knobloch, E. 1987 The Takens–Bogdanov bifurcation with $O(2)$ symmetry. *Phil. Trans. R. Soc. Lond.* A **322**, 243–279.

Deane, A., Knobloch, E. & Toomre, J. 1987 Travelling waves and chaos in thermosolutal convection. *Phys. Rev.* A **36**, 2862–2869.

Golubitsky, M. & Stewart, I. 1985 Hopf bifurcation in the presence of symmetry. *Arch. Rat. Mech. Anal.* **87**, 107–165.

Gough, D. O. 1989 The linear theory of stellar oscillations. In *Astrophysical Fluid Dynamics* (ed. J. P. Zahn & J. Zinn-Justin). Elsevier.

Gough, D. O., Moore, D. R., Spiegel, E. A. & Weiss, N. O. 1976 Convective instability in a compressible atmosphere II. *Astrophys. J.* **206**, 536–542.

Graham, E. 1975 Numerical simulation of two-dimensional compressible convection. *J. Fluid Mech.* **70**, 689–703.

GUCKENHEIMER, J. & HOLMES, P. 1983 *Nonlinear Oscillations, Dynamical Systems and Bifurcations of Vector Fields*. Springer.

HUGHES, D. W. & PROCTOR, M. R. E. 1988 Magnetic fields in the solar convection zone: magnetoconvection and magnetic buoyancy. *Ann. Rev. Fluid Mech.* **20**, 187–223.

HURLBURT, N. E. & TOOMRE, J. 1988 Magnetic fields interacting with nonlinear compressible convection. *Astrophys. J.* **327**, 920–932.

HURLBURT, N. E., TOOMRE, J. & MASSAGUER, J. M. 1984 Two-dimensional compressible convection extending over multiple scale heights. *Astrophys. J.* **282**, 557–573.

HURLBURT, N. E. & WEISS, N. O. 1987 Interaction between magnetic fields and convection. In *The Role of Fine-Scale Magnetic Fields on the Structure of the Solar Atmosphere* (ed. E.-H. Schröter, M. Vázquez & A. A. Wyller), pp. 35–46. Cambridge University Press.

KNOBLOCH, E. 1986 On convection in a horizontal magnetic field with periodic boundary conditions. *Geophys. Astrophys. Fluid Dyn.* **36**, 161–177.

KNOBLOCH, E., DEANE, A. E., TOOMRE, J. & MOORE, D. R. 1986 Doubly diffusive waves. *Contemp. Maths* **56**, 203–216.

LAMB, H. 1932 *Hydrodynamics* (6th edn). Cambridge University Press.

MOSS, D. L. 1986 Magnetic fields in stars. *Phys. Rep.* **140**, 1–74.

NAGATA, W. 1986 Symmetric Hopf bifurcations and magnetoconvection. *Contemp. Maths* **56**, 237–265.

NAGATA, M., PROCTOR, M. R. E. & WEISS, N. O. 1989 Transitions to asymmetry in magnetoconvection. *Geophys. Astrophys. Fluid Dyn.* (in press).

NORDLUND, Å. 1984 Magnetoconvection: the interaction of convection and small scale magnetic fields. In *The Hydromagnetics of the Sun* (ed. T. D. Guyenne), pp. 37–46. ESA SP-220.

NORDLUND, Å. 1985 Solar convection. *Solar Phys.* **100**, 209–235.

PARKER, E. N. 1984 Alfvén waves in a thermally stratified fluid. *Geophys. Astrophys. Fluid Dyn.* **29**, 1–12.

PRIEST, E. R. 1982 *Solar Magnetohydrodynamics*. Reidel.

PROCTOR, M. R. E. 1986 Columnar convection in double-diffusive systems. *Contemp. Maths* **56**, 267–276.

PROCTOR, M. R. E. & WEISS, N. O. 1982 Magnetoconvection. *Rep. Prog. Phys.* **45**, 1317–1379.

RAND, D. 1982 Dynamics and symmetry: predictions for modulated waves in rotating fluids. *Arch. Rat. Mech. Anal.* **79**, 1–37.

ROSSBY, H. T. 1969 A study of Bénard convection with and without rotation. *J. Fluid Mech.* **36**, 309–335.

RUELLE, D. 1973 Bifurcations in the presence of a symmetry group. *Arch. Rat. Mech. Anal.* **51**, 136–152.

SPIEGEL, E. A. 1965 Convective instability in a compressible atmosphere I. *Astrophys. J.* **141**, 1068–1090.

STEWART, I. N. 1988 Bifurcations with symmetry. In *New Directions in Dynamical Systems* (ed. T. Bedford & J. W. Swift), pp. 233–283. Cambridge University Press.

WALDEN, R. W., KOLODNER, P., PASSNER, A. & SURKO, C. M. 1985 Travelling waves and chaos in convection in binary fluid mixtures. *Phys. Rev. Lett.* **55**, 496–499.

WEISS, N. O. 1981*a* Convection in an imposed magnetic field. Part 1. The development of nonlinear convection. *J. Fluid Mech.* **108**, 247–272.

WEISS, N. O. 1981*b* Convection in an imposed magnetic field. Part 2. The dynamical regime. *J. Fluid Mech.* **108**, 273–289.

WEISS, N. O. 1981*c* The interplay between magnetic fields and convection. *J. Geophys. Res.* **86**, 11689–11694.